Plagioclase, orthopyroxene, clinopyroxene, glass magma-meter and application to Mount

Ruapehu, New Zealand and Paraná volcanic province, Brazil


by

Lydia Jane Harmon


Master's Thesis

Submitted to the Faculty of the

Graduate School of Vanderbilt University

in partial fulfillment of the requirements

for the degree of


MASTER OF SCIENCE

in


Earth and Environmental Sciences

August 2016

Nashville, Tennessee


Approved:

Guilherme A. R. Gualda, Ph.D.

Lily L. Claiborne, Ph.D.

ACKNOWLEDGEMENTS

# TABLE OF CONTENTS

LIST OF TABLES

LIST OF FIGURES

**Introduction and Motivation:**

Understanding the storage conditions of magma bodies is essential when interpreting magma

evolution, crystallization, and eruption. The storage conditions affect fundamental aspects of

magma crystallization, particularly the crystallizing assemblage (Lange et al, 2009; Waters and

Lange, 2015; Wark and Watson, 2006; Putirka, 2008; Holland and Powell, 2006; Blundy et al,

2008). Determining storage conditions for intermediate magmas is especially important, as the

conditions influence the style of eruption (i.e. explosive or effusive), and they can impact magma

eruptibility (i.e. internal or external eruption triggers; Tramontano et al, 2016 ).

In the quest for determining storage conditions, we focus on understanding storage pressure,

temperature, fluid ($H_2O$ wt%) content, and oxygen fugacity ($f_{O2}$). Determining crystallization

pressure and temperature is the primary goal, as these parameters affect mineral stability, fluid

and volatile stability, and exsolution. Additionally, they control the physical behavior of

magmas, and pressure is proxy for the depth of crystallization. The water activity affects mineral

stability, and greatly affects magmatic properties, so fluid content, modeled as $H_2O$ wt%, is a

critical parameter to estimate for volcanic systems. The $f_{O2}$ controls the ratio of ferric to ferrous

iron, and thus influences the stable crystallizing mineral assemblage, which is important in

systems containing mafic minerals (Lange and Carmichael, 1987; Toplis and Carrol, 1995;

Liebske et al., 2002, Sack et al., 1980; Kilinc et al., 1983; Mysen et al., 1985; Mysen, 1990;

Kress and Carmichael, 1991; Moore et al., 1995; Baker and Rutherford, 1996).

The focus of this study is on constraining storage conditions of intermediate-composition

volcanic systems (i.e. andesites to dacites). Intermediate magmas erupt over a wide range of

sizes from small cone volcanoes to caldera-scale eruptions (e.g. Paraná volcanic province)

(Gravely et al, 2015), and over a range of eruptive styles from lava flows to explosive plinian

eruptions (Cashman and Giordano, 2014). Intermediate systems are inherently diverse both in eruptive style and scale, thus making them important magmas to understand from a volcanological and petrological standpoint.

Several methods exist to estimate crystallization conditions of intermediate magmas, e.g. based on Ti-Fe oxide equilibria (Sack and Ghiorso, 1991; Ghiorso and Evans, 2008), abundance of trace elements in minerals, e.g. Ti in Zircon, Zr in rutile (Wark and Watson, 2006; Ferry and Watson, 2007), and $H_2O$-$CO_2$ equilibria (Moore, 2008; Moore and Carmichael, 1998; Liu et al, 2005). Putirka (2008) summarizes the many efforts in geothermobarometry, but points out the large uncertainties associated with previous geobarometry work. Our method aims to reduce these large pressure uncertainties.

A recent approach by Gualda and Ghiorso (2014) utilizes the compositional thermodynamics tool rhyolite-MELTS (Gualda and Ghiorso, 2015) to model the storage pressures for silicic systems bearing glass in equilibrium with quartz and two feldspars (qtz+2feldspars) (Gualda and Ghiorso, 2014). The present study follows and expands upon their methodology to propose a similar method that can be applied to rocks containing glass, plagioclase, and two pyroxenes. This method finds applications primarily in compositionally intermediate magmas whose major mineral assemblages are commonly characterized by plagioclase and two pyroxenes, namely orthopyroxene and clinopyroxene. We demonstrate that, in addition to pressure, rhyolite-MELTS can inform us about maximum crystallization temperature, $H_2O$ wt% of the melt, and the $f_{O2}$ of the system – thus we call it a "magma-meter".

The magma-meter utilizes the composition of glass coexisting with the plagioclase, orthopyroxene, and clinopyroxene (plag+opx+cpx) minerals in natural pumice samples. Pumice is particularly useful, as it represents the pre-eruptive crystallizing magma assemblage, whose

glass retains the pre-eruptive melt composition. Importantly, pumice represents a cohesive parcel of magma that did not fragment during eruption. The crystals in contact with the volcanic glass are the same crystals that were forming from the magmatic melt, so we infer that the glass is in equilibrium with the crystal neighbors. Using pumice, the magma-meter employs the computational thermodynamics software rhyolite-MELTS to calculate the condition under which crystallizing assemblage, plag+opx+cpx, is saturated and in equilibrium with a melt with composition equal to that of the natural glass (for details, see Gualda and Ghiorso, 2014). The magma-meter was tested against results from experiments retrieved from the literature. We apply the magma-meter to two natural plag+opx+cpx-bearing systems. First, we apply the magma-meter to a well-studied, currently active system – Mt Ruapehu in the southern Taupo Volcanic Zone (TVZ), New Zealand (Hackett and Houghton, 1989; Rowland et al, 2010).  Mt Ruapehu is structurally well-understood volcano in the southern TVZ, one of the most currently active volcanic zones in the world (Wilson et al, 1995); it thus serves as a methodological testing ground for the magma-meter. We also apply the magma-meter to the Palmas unit of the Paraná igneous province, southern Brazil, for which estimates of crystallization conditions are either lacking or plagued by very large uncertainties (Nardy et al, 2011; Bryan et al, 2010). Bryan et al (2010) suggested that Paraná volcanic deposits represent some of the largest eruptions in the geological record –including several super-eruptions with erupted volumes that exceeded 5,000 $km^3$ per eruption.

**The Magma-Meter:**

Using rhyolite-MELTS, we model the crystallizing magma from liquidus (0% crystalline) to near-solidus (~90% crystalline) in order to determine the pressure-temperature conditions necessary to satisfy the set of conditions for which plag+opx+cpx phases are simultaneously

stable for a given melt composition. Because the input melt composition is the target

composition, we search for the conditions under which plag+opx+cpx are in equilibrium with

melt at its liquidus.
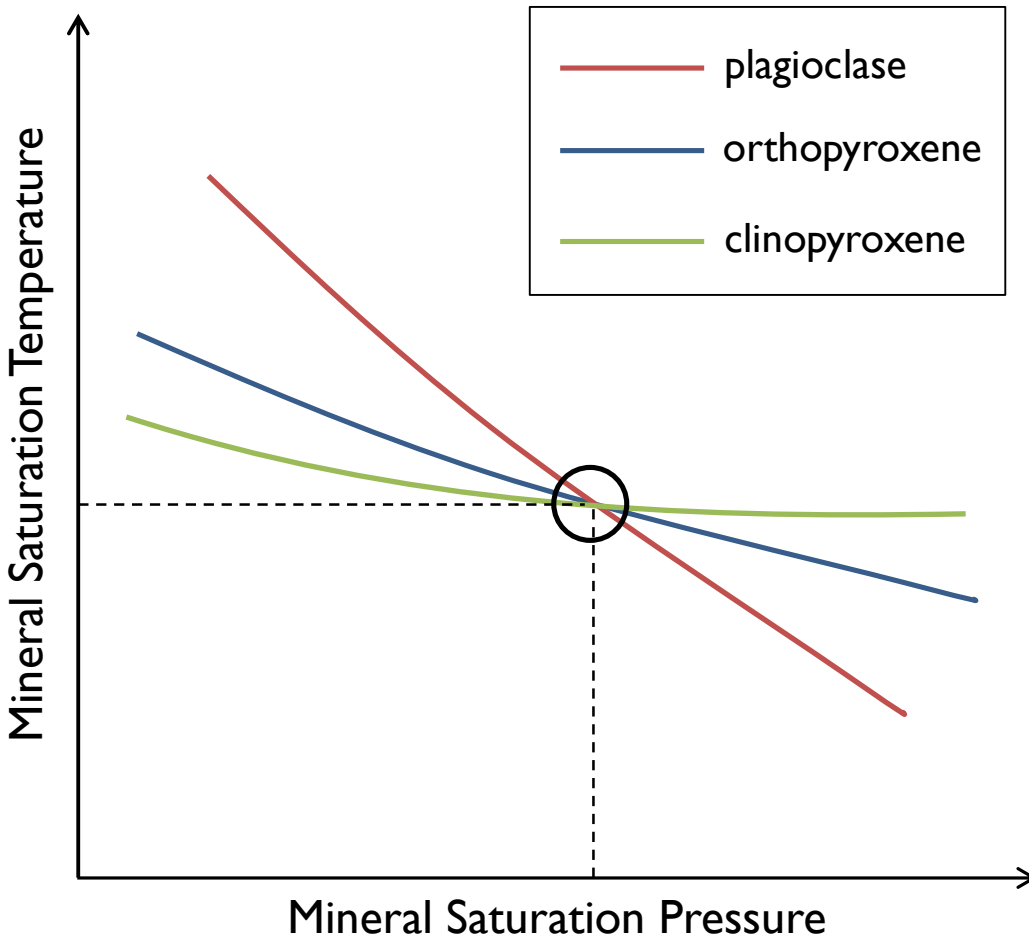


**Figure 1.** Principle of the magma-meter, adapted from Gualda and Ghiorso, 2014. The three curves represent the saturation conditions for the three mineral phases in pressure-temperature space for a given melt composition. Rhyolite-MELTS can be used to calculate saturation curves like this for any given melt composition. The circle marks the "triple-junction", the point at which the three curves cross, which is the only point at which all three phases are in simultaneous equilibrium with the input melt composition. The saturation temperature and pressure are the conditions for which the melt is in equilibrium with the three mineral phases, and thus represent the storage conditions of the magma.

First, we calculate the mineral stability in temperature-pressure space in order to model the

saturation curve for each individual phase (plag, opx, and cpx). As seen in Figure 1, equilibrium

requires that the three mineral phase-in saturation curves cross at a single point, which represents the specific pressure and temperature conditions at which these three minerals are in equilibrium with the melt. There is only a single pressure-temperature condition at which equilibrium is possible, as the composition of the melt would have to change if either the pressure or temperature changed, unless the glass represents a eutectic composition. This single point where all three phases are saturated is referred to here as the "triple-junction". For a more complete description of the concept, please refer to Gualda and Ghiorso (2014).

In addition to exploring equilibrium pressures and temperatures, we also studied the effects of $H_2O$ content and $f_{O2}$. Gualda and Ghiorso (2014) investigated the effect of $H_2O$ content on the calculated pressures (and temperatures) for the assemblage quartz+2feldspars, and showed that the effect is rather modest. For assemblages in which Fe-bearing minerals are abundant, it is important to also consider the effect of $f_{O2}$, given that ferrous-ferric ratio controls, directly or indirectly, the stability of mafic minerals.

To model the storage pressures, the steps below were carried out for each glass composition:

1. We first explored plag+opx+cpx stability in pressure-temperature space. The pressure was varied from 400 MPa to 25 MPa using a coarse 25 MPa pressure step. For each pressure step, the system was modeled from liquidus (~ 1200 ℃ and 0% crystalline) to near solidus (~700 ℃ and 90% crystalline) in 1 ℃ temperature steps. Rhyolite-MELTS automatically determines the liquidus temperature for each pressure step, and it interrupts the temperature sequence once the percentage of solids is above 90 wt. %. The result of a sequence of calculations like this is a collection of saturation surfaces (see Figure 1). These calculations are performed with $H_2O$ and $f_{O2}$ held constant.

2. We then considered the effect of $H_2O$ on the system. For each composition, we consider water contents from ~$H_2O$ saturated to ~3 wt% below $H_2O$ saturation, in 1 $H_2O$ wt% steps, as determined by rhyolite-MELTS.

3. Since the plag+opx+cpx assemblage is sensitive to oxygen fugacity, we also tested the sensitivity of $f_{O2}$ on the crystallizing plag+opx+cpx system. Again, for each $H_2O$ content, we explore a range of expected shallow crustal $f_{O2}$ values, from 0 to +2 $\Delta$QFM in 0.5 $\Delta$QFM steps, with some samples tested from 0 to +4 $\Delta$QFM. For each $f_{O2}$ value and $H_2O$ content, we perform the same sequence of pressure-temperature calculations described above.

A total of 12 model runs are required to constrain the storage pressure of the plag+opx+cpx assemblage in equilibrium with the melt composition. After the initial survey described above, we refine the results, by reducing the pressure steps from 25 MPa to 5 MPa, and using a smaller pressure range of 100 MPa, in order to determine a more specific crystallization pressure. The smaller $f_{O2}$ interval, in 0.5 $\Delta$QFM steps instead of 1 $\Delta$QFM steps, was necessary as the model was particularly sensitive to $f_{O2}$.

*Pressure Calculations and Limitations:*

To calculate the triple-junction pressure, we plot the saturation temperature point of each individual plag, opx, cpx phase for each modeled pressure, Figure 2. Each curve connects the phase-in saturation temperature points for an individual mineral phase. As the three discretized phase-in curves rarely cross exactly, the triple-junction is calculated from the "residual temperature" by finding the difference in saturation temperatures between the first (highest temperature) and last (lowest temperature) between plag, opx, cpx, Figure 2. As the three phases

saturate at more similar temperatures, the residual temperature decreases until it reaches the triple-junction, before increasing as the saturation temperatures for plag, opx, and cpx diverge.
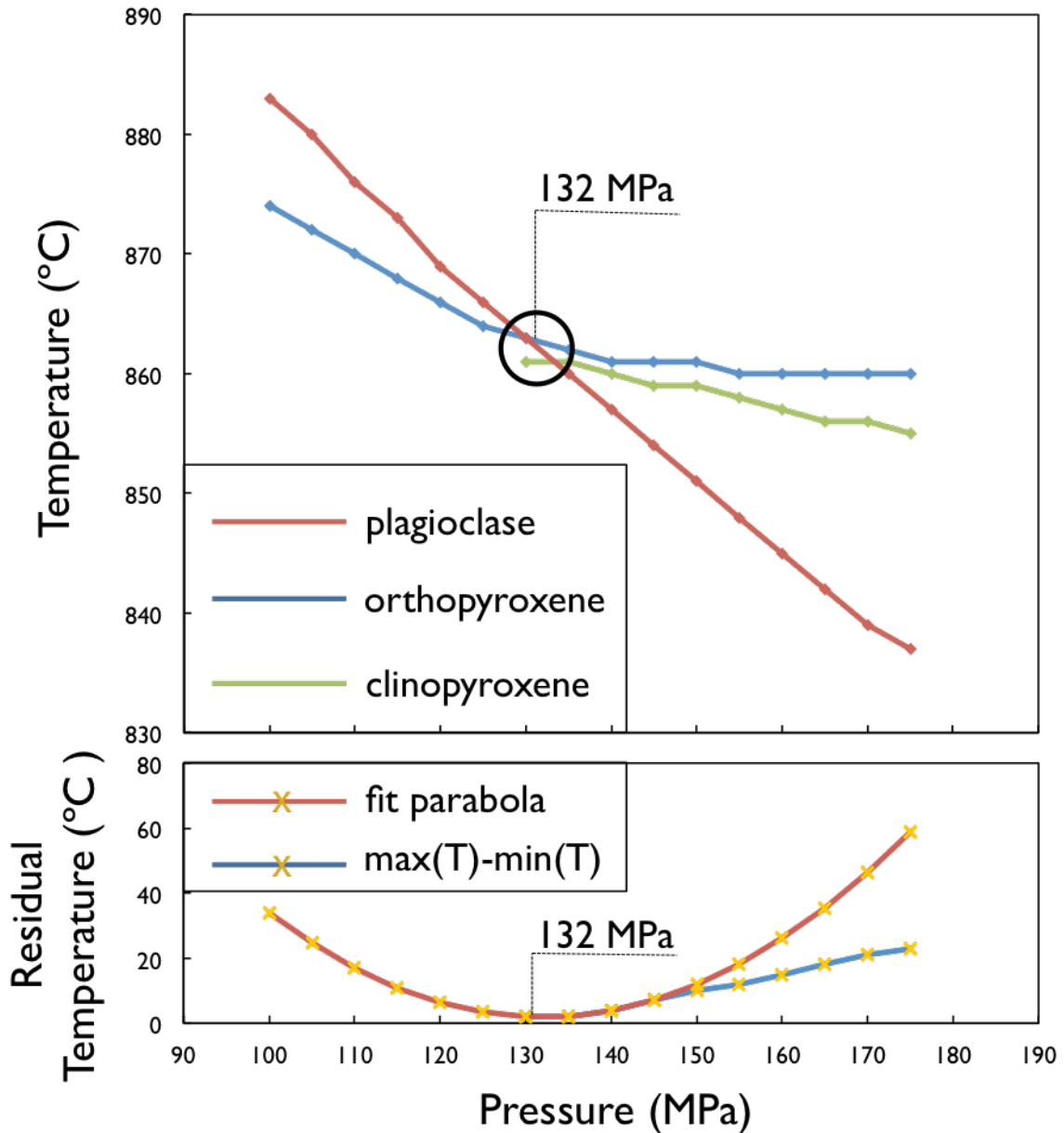


**Figure 2.** Example of an application of the magma-meter. The saturation curves were calculated in pressure-temperature space, under water saturated conditions and with $f_{O2}$ equal to +1 $\Delta$QFM (top panel). To find the triple-junction (bottom panel), we calculate a residual temperature curve as the difference between the maximum saturation temperature (max(T)) and minimum saturation temperature (min(T)) for each pressure. We then fit a parabola to the 5 points surrounding the minimum of the max(T)-min(T) to find the best estimate of crystallization pressure. For details, see text.

The magma-meter calculation is deemed successful if the residual temperature reaches ≤8 ºC. If the residual temperature never goes below 8 °C, we conclude that there is no set of conditions under which the plag+opx+cpx can be in simultaneous equilibrium with a melt of the given composition. The 8 ºC threshold is somewhat arbitrary, but our tests suggest it is a good compromise between locating a viable triple-junction and excluding spurious results. Because we use discretized pressure steps of 5 MPa, it is unlikely that we have sampled the exact plag+opx+cpx saturation pressure. To obtain the estimated storage pressure, we interpolate between pressure calculations to find the minimum residual temperature. We fit a parabola to 5 data points: the minimum in residual temperature, and two pressure steps above and below the minimum residual temperature, Figure 2. This procedure is described in more detail in Gualda and Ghiorso (2014).

In most of our Mt Ruapehu samples, clinopyroxene undergoes a phase change at pressures slightly below the triple-junction. In many of these cases, it is inaccurate to fit a parabola to the two data points at pressures below the minimum in residual temperature. There are two potential scenarios:

1. We calculate the estimated storage pressure based on the minimum residual temperature, two pressures above, and one pressure below the minimum residual temperature.

2. In cases where the phase change occurred right below the minimum residual temperature, a parabola could not be fit. In this instance, the estimated pressure was simply the pressure corresponding to the minimum in residual temperature.

Of the 13 Mt Ruapehu ranked method samples that produced a minimum residual temperature ≤ 8 ºC, 5 samples required a pressure estimate based on the residual temperature.

For application to rocks that are only two-phase bearing i.e. contain only plag+opx, plag+cpx, or opx+cpx, the pressure estimate is calculated based on the plag+pyroxene or opx+cpx "double-junction" instead of the plag+opx+cpx triple-junction. While this method is useful for rocks with only two phases present, the double-junction inherently carries a larger error, as the residual temperature (and successive pressure estimate) is based on the intersection of two curves instead of three (see Gualda and Ghiorso, 2014). Since all three plag+opx+cpx phases are present in the samples for this study, the magma-meter calculations that only produced a double-junction were disregarded. However, for rocks bearing only two of the three plag+opx+cpx phases, this two-phase magma-meter method would be useful.

*An Example:*

We demonstrate the methods of the magma-meter using one of the successfully modeled Mt Ruapehu samples, sample X262AD. The method described above was applied to all Ruapehu averaged glass analyses. Figure 3 shows the results for all of the $H_2O$ wt% and $f_{O2}$ model conditions calculated for that sample. It can be seen that the plag+opx+cpx phase assemblage is sensitive to the choice of $f_{O2}$ and $H_2O$ content, with viable plag+opx+cpx triple-junctions resulting only for a narrow range of $f_{O2}$ ($\Delta QFM = +1$) and $H_2O$ content (water saturated). In Figure 2, we show the more detailed rhyolite-MELTS calculation performed with 5 MPa steps at +1 $\Delta QFM$ and $H_2O$ saturated. From these results, we calculate the estimated crystallization pressure of 132 MPa.
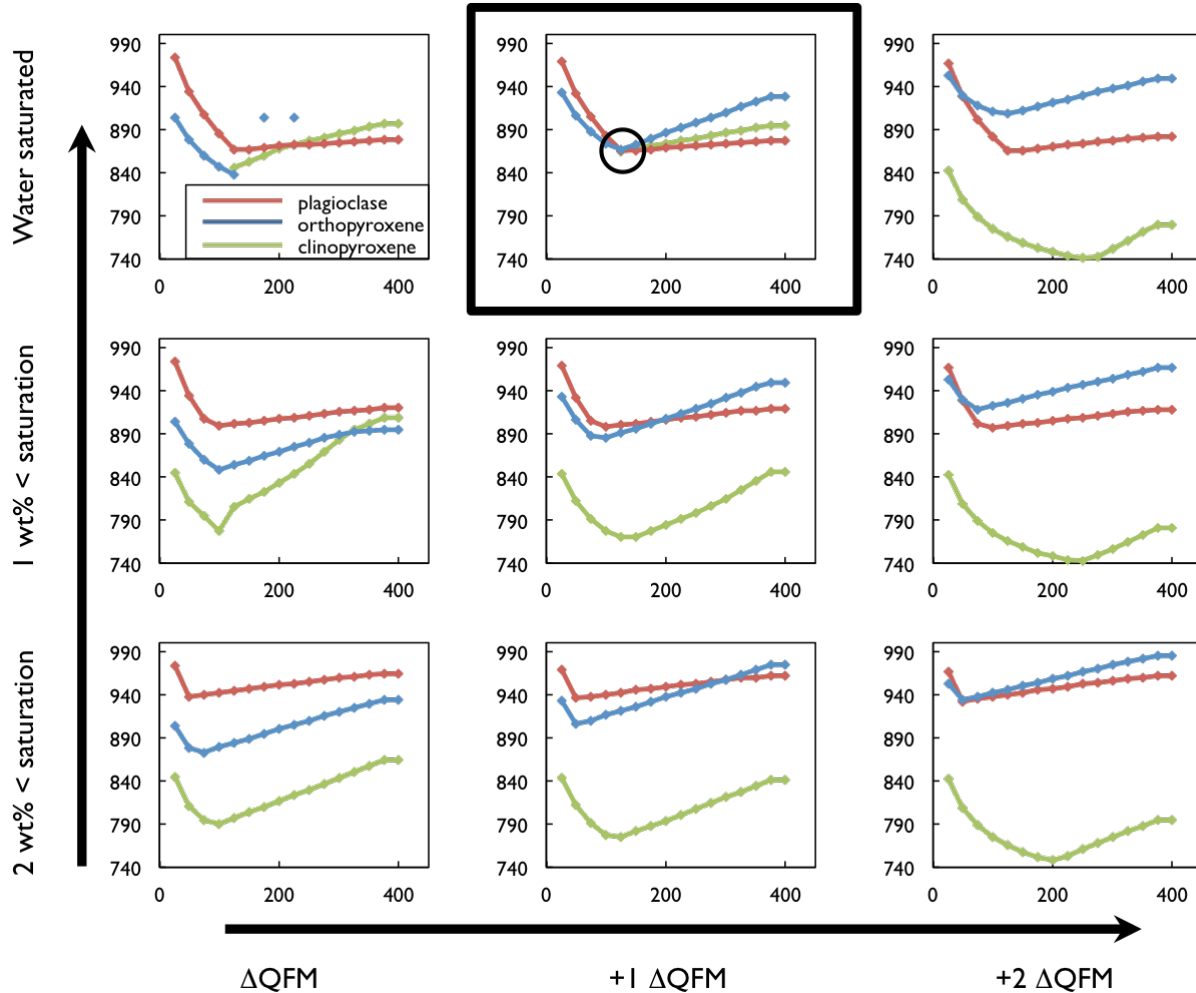
**Figure 3.** Magma-meter results detailing the effects of $f_{O2}$ and $H_2O$ wt% on triple-junction viability. We modeled a suite of rhyolite-MELTS calculations on a single melt composition (sample X262AD) from water saturated to 2 wt% below saturation in 1 wt% steps (shown on y-axis), and from $\Delta$QFM to +2 $\Delta$QFM in 1 $\Delta$QFM steps (shown on x-axis). For each distinct $f_{O2}$ and $H_2O$ condition, the model was run from 1200 – 700 ºC in 1 ºC steps and from 400-25 MPa in 25 MPa steps. When the plag+opx+cpx saturation curves saturated within 8 ºC, a triple-junction was calculated. Of all the conditions, the only one to calculate a triple-junction was modeled at +1 $\Delta$QFM and was water saturated (top-center panel). The $H_2O$ and $f_{O2}$ parameters indicate the storage conditions of the magma, since these are the only conditions which produce a triple-junction. This modeling process was repeated for 43 melt compositions which calculated triple-junctions for water saturated and +1 $\Delta$QFM conditions. For all samples, we modeled the samples at water saturated conditions and +1 $\Delta$QFM.

Our magma-meter differs from the qtz+2feldspar geobarometer (Gualda & Ghiorso, 2014) in that we tested the full range of $f_{O2}$ values to determine mineral stability. Additionally, the triple-junction saturation is calculated only when the plag+opx+cpx assemblage is in equilibrium within 8 ºC of all three phase-in curves. We discarded samples that did not meet the plag+opx+cpx 8 ºC saturation requirement.

For a more detailed account of calculating the point at which all three are stable, please refer to Gualda & Ghiorso, 2014.

**Application to Experiments:**

The experimental glass compositions were taken from the Library of Experimental Phase

Relations (LEPR) database. We chose the experiments based on mineral assemblage

(plag+opx+cpx-bearing), pressure (upper crustal pressures <1 GPa), and water-content

(documented wt. % $H_2O$ in the samples). We modeled 8 experimental glass compositions from

the LEPR database that were taken from several different experiments, detailed in Table 1.
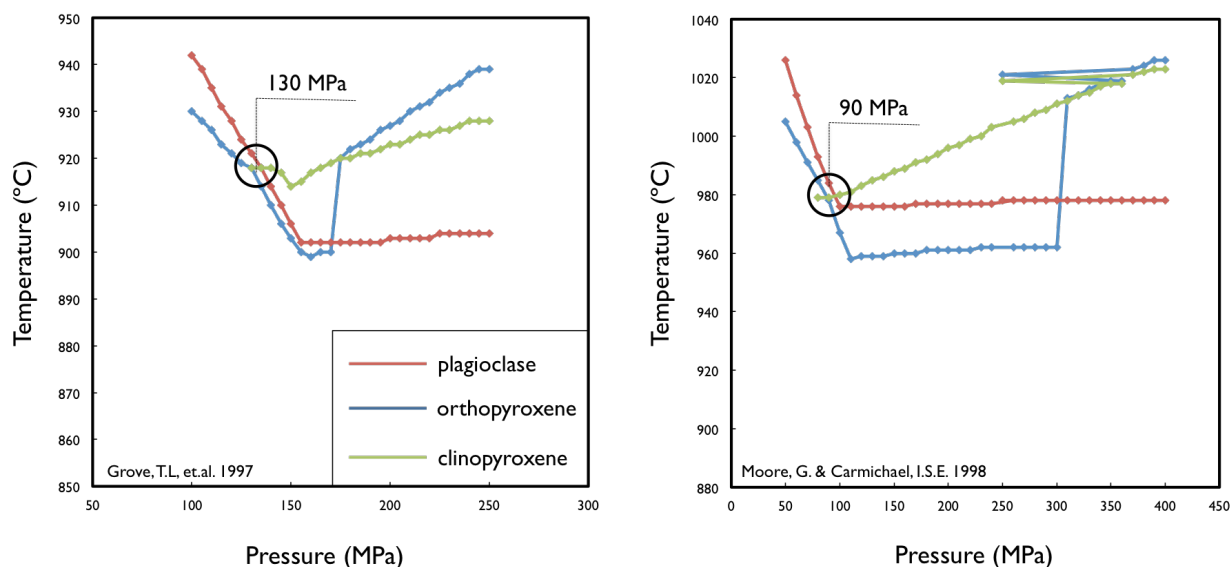


**Figure 4.** Magma-meter results of experiments from the literature (Grove T.L. et al, 1997; Moore G. and Carmichael I.S.E., 1998) . The two experiments were plag+opx+cpx bearing and run at 100 MPa with fO2 = NNO and +1.1 NNO, respectively, and with 4.9 wt% water and 3.6 wt% water in the system, respectively. The results show that when the magma-meter calculates a triple-junction, the results are valid.

Of the 8 compositions tested, 2 yielded viable triple-junction calculations using the magma-

meter, Table 2. Overall, the experimental glass compositions that had substantial water in the

system and that were conducted at lower pressures (< 200 MPa) yielded results, or were closer to

yielding a triple-junction. In Figure 4, the two successful experimental compositions are

highlighted. The rhyolite-MELTS qtz+2feldspar geobarometer is notoriously sensitive to the

quality of the glass compositions, which helps to resolve why only 2 compositions yielded

| Sample | Experiment | Author (year) | Laboratory | Device | T (C) | P (MPa) | fO2 cond | Phases |
|---|---|---|---|---|---|---|---|---|
| LEPR_Index_1426 | PIN98s | Prouteau, G., Scaillet, B. (2003) | Universite de Bretagne Occidentale | IHPV | 950 | 400 | NNO+3.2 | liq+plag+cpx+spn+opx |
| LEPR_Index_1622 | 8 | Kawamoto, T. (1996) | University of Tokyo | PC | 975 | 500 | NNO+1.3 | cpx+opx+plag+spn |
| LEPR_Index_3603 | PEM12-11 | Moore, G., and Carmichael, I.S.E. (1998) | UC-Berkeley | IHPV | 1000 | 44 | NNO+2.8 | liq+opx+plag+ox+cpx |
| LEPR_Index_3607 | PEM12-19 | Moore, G., and Carmichael, I.S.E. (1998) | UC-Berkeley | IHPV | 975 | 100.8 | NNO+1.1 | liq+opx+plag |
| LEPR_Index_4037 | TJ-34 | Auwera, J. V., and Longhi, J. (1994) | Lamont-Doherty Earth Observatory | 1-atm | 1085 | 0.1 | NNO | liq+plag+opx+cpx+ilm+spn |
| LEPR_Index_4799 | 1140mf #27 | Grove, T.L., Donnelly-Nolan, J.M., Housh, T. (1997) | MIT | CSPV | 940 | 100 | NNO | liq+opx+cpx+plag+spn |
| LEPR_Index_4801 | 1140mf #29 | Grove, T.L., Donnelly-Nolan, J.M., Housh, T. (1997) | MIT | CSPV | 910 | 100 | NNO | liq+opx+cpx+plag+spn |
| LEPR_Index_4806 | 1140mf #41 | Grove, T.L., Donnelly-Nolan, J.M., Housh, T. (1997) | MIT | CSPV | 915 | 150 | NNO | liq+opx+cpx+plag+spn |

**Table 1.** LEPR experiment conditions tested by the magma-meter. All experiments are < 1 GPa.

| Sample | Magma-Meter Results | | Magma-Meter Parameters | | | | |
|---|---|---|---|---|---|---|---|
| | P (MPa) | T (ºC) | P Range (MPa) | P step (MPa) | T Range (ºC) | fO2 (Δ NNO) | H2O (wt %) |
| LEPR_Index_1426 | - | - | 500-5 | 5 | 1200-700 | NNO+3.2 | 5.46 |
| LEPR_Index_1622 | - | - | 400-50 | 50 | 1200-700 | NNO+1.3 | 0.00 |
| LEPR_Index_3603 | - | - | 500-5 | 5 | 1200-700 | NNO+2.8 | 0.80 |
| LEPR_Index_3607 | 100 | 975 | 400-50 | 10 | 1200-700 | NNO+1.1 | 3.60 |
| LEPR_Index_4037 | - | - | 500-5 | 5 | 1200-700 | NNO | 0.00 |
| LEPR_Index_4799 | 140 | 920 | 500-5 | 5 | 1200-700 | NNO | 4.90 |
| LEPR_Index_4801 | - | - | 500-5 | 5 | 1200-700 | NNO | 0.00 |
| LEPR_Index_4806 | - | - | 500-5 | 5 | 1200-700 | NNO | 0.00 |

| Sample | Composition | | | | | | | | | | | | | |
|---|---|---|---|---|---|---|---|---|---|---|---|---|---|---|
| | SiO2 | TiO2 | Al2O3 | Fe2O3 | Cr2O3 | FeO | MnO | MgO | NiO | CoO | CaO | Na2O | K2O | H2O |
| LEPR_Index_1426 | 71.65 | 0.24 | 15.26 | 0.00 | 0.00 | 2.08 | 0.07 | 1.00 | 0.00 | 0.00 | 2.99 | 4.50 | 2.20 | 5.46 |
| LEPR_Index_1622 | 63.50 | 0.35 | 18.90 | 3.00 | 0.00 | 0.00 | 0.00 | 2.96 | 0.00 | 0.00 | 5.30 | 4.44 | 0.74 | 0.00 |
| LEPR_Index_3603 | 51.40 | 0.93 | 3.20 | 2.01 | 0.00 | 6.58 | 0.00 | 16.30 | 0.00 | 0.00 | 20.70 | 0.30 | 0.02 | 0.80 |
| LEPR_Index_3607 | 61.80 | 0.61 | 16.50 | 0.00 | 0.00 | 3.77 | 0.00 | 1.70 | 0.00 | 0.00 | 4.91 | 3.50 | 1.87 | 3.60 |
| LEPR_Index_4037 | 60.70 | 2.34 | 13.20 | 0.00 | 0.00 | 7.25 | 0.16 | 2.98 | 0.00 | 0.00 | 5.77 | 2.79 | 2.20 | 0.00 |
| LEPR_Index_4799 | 62.39 | 0.80 | 15.69 | 0.00 | 0.00 | 3.93 | 0.08 | 1.32 | 0.00 | 0.00 | 3.42 | 4.76 | 2.43 | 4.90 |
| LEPR_Index_4801 | 51.10 | 0.87 | 3.38 | 0.00 | 0.03 | 10.80 | 0.34 | 14.40 | 0.00 | 0.00 | 18.90 | 0.35 | 0.00 | 0.00 |
| LEPR_Index_4806 | 51.00 | 0.77 | 2.50 | 0.00 | 0.00 | 12.60 | 0.37 | 14.00 | 0.00 | 0.00 | 18.50 | 0.36 | 0.00 | 0.00 |

**Table 2.** LEPR magma-meter results (top) and compositions (bottom).

triple-junctions in our experimental calculations. The geobarometer is so sensitive to glass

compositions that previous studies have used the geobarometer to pick quality glass samples

(Gualda and Ghiorso, 2014; Begue et al, 2014; Pamukcu et al, 2015).

**Application to Natural Systems – Mt Ruapehu:**

We applied the magma-meter to pumice from Mt Ruapehu, a relatively small, andesite in

composition, and highly active volcano in the southernmost section of the Taupo Volcanic Zone

(TVZ), New Zealand. The TVZ has been active for the last 2 million years, and it has produced

over 10,000 km$^3$ of erupted magma in the last 1 million years (Wilson et al, 1995; Rowland et al,

2001; Rowland et al, 2010). As well as being one of the most active volcanic regions in the

world, the TVZ is also one of the most well studied volcanic zones. The highly active Mt

Ruapehu erupts explosively, with the most recent major eruption in 1996.
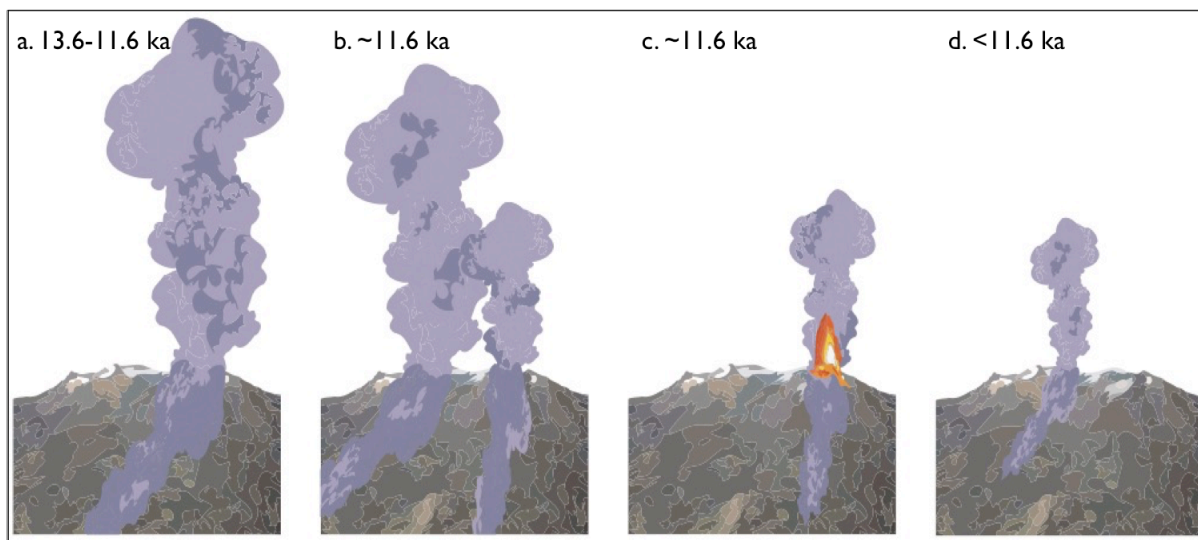


**Figure 5.** Schematic of Mt Ruapehu eruption sequence through time inferred from the PDC deposits, adapted from Cowlyn (2016). a) From 13.6 to 11.6 ka, PDC units 1-3 erupted from the North Crater. This period ended with smaller PDC units 11-12. b) at ~11.6 ka, an explosive eruption created the South Crater and deposited PDC unit 4. Concurrently, the North Crater erupted PDC unit 5. c) a more energetic fire fountaining eruption caused the welded PDC unit 6, and PDC unit 7. d) from >11.6 ka, the South vent continued to erupt, but the magmatic activity changed to a subplinian/vulcanian style, and emplaced PDC units 8-10.

Mt Ruapehu has been active for ~250 ka and it has erupted from multiple different vents throughout its history (Hackett and Houghton, 1989; Cowlyn, 2016). The progression of eruptive conditions and vents over the last 13.6 ka was detailed by Cowlyn (2016), Figure 5. We apply the magma-meter to Mt Ruapehu to better constrain pre-eruptive storage conditions, using samples collected during extensive recent fieldwork, which focused on the volcanology of recent pyroclastic deposits (Cowlyn, 2016).

*Samples:*

The samples investigated in this study are from 12 pyroclastic density current (PDC) deposits erupted and deposited proximally to Mt Ruapehu's eastern flank ≤ 13.6 ka. All stratigraphic, textural, and volcanological work is based on field and lab work by James Cowlyn (Cowlyn, 2016). The 12 units can be categorized stratigraphically (and temporally) as follows, as detailed in Figure 5:

1. Units 1-3: From ~13.6 to 11.6 ka, Mt Ruapehu's largest plinian deposits, the Ohinewairua PDC units, were erupted from the pre-existing North Crater vent

2. Units 11-12: These smaller volume PDC units from the same North Crater marked the end of the Plinian sequence (Units 1-3), evidenced by these smaller, somewhat degassed units

3. Units 4-5: At ~11.6 ka, Unit 4 excavated a new conduit, the South Crater. The syn-eruptive Unit 5 erupted from the pre-existing conduit, the North Crater.

4. Units 6-7: Also at ~11.6 ka, Units 6 and 7 erupted from the North Crater area as hotter degassed magma, which are preserved as welded tuffs.

5. Units 8-10: The youngest PDCs studied erupted < 11.6 ka, representing  a change in eruptive style to smaller subplinian/vulcanian eruptions sourced near the South Crater.

The pumice-dominated PDCs all contain glass plus plagioclase (labradorite or bytownite), clinopyroxene (augite), orthopyroxene (enstatite), and titanomagnetite, with ilmenite present in two of the samples (Cowlyn, 2016), which makes the samples viable for application to the plag+opx+cpx magma-meter. A total of 40 distinct pumice samples were utilized for this study.

*Analytical Methods - Glass Analyses:*

The glass and phenocryst compositions for the rhyolite-MELTS calculations were averaged from EDS-analyzed thin sections of individual pumice clasts by James Cowlyn.  Glass and phenocryst compositions were obtained at Vanderbilt University (Nashville, TN, USA), using an Oxford X-max 50-mm$^2$ Energy-Dispersive Spectrometer (EDS) attached to a Tescan Vega 3 LM Variable Pressure Scanning Electron Microscope (SEM). All glass and phenocryst analyses were obtained by EDS on the SEM using 15 kV accelerating voltage. Quality of the results was monitored by analyzing the reference standards Glass Mountain Rhyolite (RGM-1) and AGV Andesite in the same analytical sessions.

For each sample, we obtained 10-20 individual glass compositions, so as to minimize the effects of heterogeneities in the glass due to chemical alteration, physical imperfections, and presence of inclusions. To select glass analyses for averaging, we used the "median average deviation" (MAD) method. This technique finds the standard deviation about the median, so it is less affected by outliers than a standard deviation about the mean (for further information, see http://www.academia.edu/5324493/Detecting_outliers_Do_not_use_standard_deviation_around_ the_mean_use_absolute_deviation_around_the_median). Analyses within ±2.5 MAD were further considered. The glass analyses were averaged using two techniques: a "ranked method" and a "1% method". The ranked method ranks the glass compositions by decreasing $SiO_2$ content, and averages the analyses of highest $SiO_2$ content until >5 analyses are averaged. The

1% method ranks the glass spectra by decreasing $SiO_2$ content, and averages the glass

compositions within 1% of the maximum $SiO_2$ value.

The ranked method and 1% method intentionally bias the average compositions towards higher

$SiO_2$ content in order to compensate for the effect of plagioclase inclusions ($SiO_2$ ~65-66 wt. %),

which would artificially lower the $SiO_2$ content of the glass. At least 5 glass analyses were

averaged in order to obtain an average glass composition, Table 3.

*Results from Mt Ruapehu:*

Mt Ruapehu samples have a distribution of crystallization pressures from 54 to 148 MPa, which

implies that magma is stored in the shallow crust. The ranked method and 1% method for glass

analyses give similar results, as calculated pressures are within 5-10 MPa of one another.

For the 40 ranked method glass compositions, 13 glass compositions yield a triple-junction

pressure based on a minimum residual temperature of $\leq 8$ ºC (see above for explanation) while

for the 1% method, a total of 11 of 23 modeled glass compositions yield a triple-junction, Table

3. The two methods for calculating glass compositions return similar results, therefore we carry

the results forward with both methods. However, the 1% method was occasionally affected by

the unintentional inclusion of plagioclase in the glass analyses.

The $f_{O2}$ ranges between $\Delta QFM = +0.5$ and $\Delta QFM = +1.5$, with the majority of samples

producing a triple-junction at $\Delta QFM = 1$. We only find viable conditions for the cases in which

magma is $H_2O$ saturated at the liquidus.

 Pressures obtained from the ranked method range from 54 MPa to 148 MPa, which corresponds

to magma storage depths of $2.1 - 5.8$ km assuming a crustal density of 2600 kg/m$^3$. The majority

of calculated triple-junction pressures (11 of 13 for ranked method, 9 of 11 for 1% method)

| Sample | Magma-Meter Results | | Magma-Meter Parameters | | | | |
| --- | --- | --- | --- | --- | --- | --- | --- |
| | P (MPa) | T (ºC) | P Range (MPa) | P step (MPa) | T Range (ºC) | fO2 (ΔQFM) | H2O (wt %) |
| 129A3 GLASS TYPE 1 (Ranked Method; Banded Sample) | - | - | 175-100 | 5 | 1200-700 | 1 | 10 |
| X129AC (Ranked Method) | 148 | 839 | 175-100 | 5 | 1200-700 | 1 | 10 |
| 129A5 (Ranked Method) (subsidiary clast type, from second magma type in mingled eruption) | - | - | 175-100 | 5 | 1200-700 | 1 | 10 |
| 129A5 (1% Method) (subsidiary clast type, from second magma type in mingled eruption) | - | - | 175-100 | 5 | 1200-700 | 1 | 10 |
| X262AD (Ranked Method) | 132 | 863 | 175-100 | 5 | 1200-700 | 1 | 10 |
| X129AC (1% Method) | 143 | 843 | 175-100 | 5 | 1200-700 | 1 | 10 |
| 225CE (Ranked Method) | 140 | 868 | 175-100 | 5 | 1200-700 | 1 | 10 |
| 225CE (1% Method) | 130 | 876 | 175-100 | 5 | 1200-700 | 1 | 10 |
| 225DE (Ranked Method) | 125 | 879 | 175-100 | 5 | 1200-700 | 1 | 10 |
| 225D3 LESS VESICULAR GLASS (Ranked) | - | - | 125-5 | 5 | 1200-700 | 1 | 10 |
| 225D3 LESS VESICULAR GLASS Highest excluded | - | - | 125-5 | 5 | 1200-700 | 1 | 10 |
| 225DE (1% Method) | 120 | 885 | 175-100 | 5 | 1200-700 | 1 | 10 |
| 225-5B (Ranked Method) | 130 | 879 | 125-5 | 5 | 1200-700 | 1 | 10 |
| 225B1 (1% Method) | 107 | 900 | 125-5 | 5 | 1200-700 | 1 | 10 |
| 262-Y1 (1% Method) | 125 | 877 | 125-5 | 5 | 1200-700 | 1 | 10 |
| X262AD (1% Method) | 135 | 861 | 125-5 | 5 | 1200-700 | 1 | 10 |
| 225AC (1% Method) | 106 | 901 | 125-5 | 5 | 1200-700 | 1 | 10 |
| 225A1 (1% Method) | - | - | 125-5 | 5 | 1200-700 | 1 | 10 |
| 225AC (Ranked Method) | 110 | 896 | 125-5 | 5 | 1200-700 | 1 | 10 |
| 225A1 (Ranked Method) | - | - | 125-5 | 5 | 1200-700 | 1 | 10 |
| 225-5B (1% Method) | 125 | 882 | 125-5 | 5 | 1200-700 | 1 | 10 |
| 225D1 Highest excluded | 105 | 901 | 125-5 | 5 | 1200-700 | 1 | 10 |
| 225C1 (1% Method) | 113 | 906 | 125-5 | 5 | 1200-700 | 1 | 10 |
| 262-Y1 (Ranked Method) | 125 | 877 | 125-5 | 5 | 1200-700 | 1 | 10 |
| 13-107 (Ranked Method) | 108 | 895 | 125-5 | 5 | 1200-700 | 1.5 | 10 |
| 13-107 (1% Method) | - | - | 125-5 | 5 | 1200-700 | 1 | 10 |

| | | | | | | | |
|---|---|---|---|---|---|---|---|
| 225D3 MORE VESICULAR GLASS (Ranked Method) | 106 | 892 | 125-5 | 5 | 1200-700 | 1 | 10 |
| 259-1-2 MATRIX GLASS (Ranked Method) | - | - | 125-5 | 5 | 1200-700 | 1 | 10 |
| 259-1-2 CLAST INTERIOR (Ranked Method) | 99 | 910 | 125-5 | 5 | 1200-700 | 0.5 | 10 |
| 12-225-19A (Ranked Method) | - | - | 125-5 | 5 | 1200-700 | 1 | 10 |
| 225B1 (Ranked Method) | 101 | 901 | 125-5 | 5 | 1200-700 | 1 | 10 |
| 13-262-4 GLASS TYPE 2 (RHS) (other alternative method) | 88 | 947 | 125-5 | 5 | 1200-700 | 1.5 | 10 |
| 259-1-2 GLASS CHILLED MARGIN (Ranked Method) | 103 | 886 | 100-5 | 5 | 1200-700 | 1.5 | 10 |
| 12-225-19A BULK (All 5 analyses) | - | - | 100-5 | 5 | 1200-700 | 1 | 10 |
| 225C1 (Ranked Method) | 118 | - | 100-5 | 5 | 1200-700 | 1.5 | 10 |
| RING PLAIN M1 LIGHT SEPARATE (Ranked Method) | - | - | 100-5 | 5 | 1200-700 | 1 | 10 |
| 225D3 MORE VESICULAR BULK (All 3 Analyses) | - | - | 100-5 | 5 | 1200-700 | 1 | 10 |
| 13-262-4 GLASS TYPE 2 (RHS) (Ranked Method) | 88 | 948 | 100-5 | 5 | 1200-700 | 1.5 | 10 |
| 13-262-4 GLASS TYPE 1 (LHS) (Ranked Method) | 54 | 971 | 100-5 | 5 | 1200-700 | 1 | 10 |
| 13-262-4 GLASS TYPE 1 (LHS) (1% Method) | 55 | 972 | 100-5 | 5 | 1200-700 | 1 | 10 |
| 225D1 (Ranked Method) | 100 | 905 | 100-5 | 5 | 1200-700 | 1 | 10 |
| 129A3 GLASS TYPE 2 (Ranked Method, Banded Sample) | - | - | 100-5 | 5 | 1200-700 | 1 | 10 |
| 129A3 GLASS TYPE 2 (1% Method, Banded Sample) | - | - | 100-5 | 5 | 1200-700 | 1 | 10 |
| 12-225-19A (1% Method) | - | - | 200-75 | 5 | 1200-700 | 1 | 10 |
| 108A1 GLASS BETWEEN MICROLITES (Ranked Method) | - | - | 100-5 | 5 | 1200-700 | 1 | 10 |
| 108A1 GLASS BETWEEN MICROLITES (1% Method) | - | - | 100-5 | 5 | 1200-700 | 1 | 10 |
| 108A1 BULK GROUNDMASS (All 5 analyses) | - | - | 200-75 | 5 | 1200-700 | 1 | 10 |
| 161A1 GLASS BETWEEN MICROLITES (Ranked Method) | - | - | 200-75 | 5 | 1200-700 | 1 | 10 |
| 109AC GLASS SITES 8-9 (Ranked Method, all 10 analyses) | - | - | 200-75 | 5 | 1200-700 | 1 | 10 |

| | | | | | | | |
|---|---|---|---|---|---|---|---|
| X108AD (Ranked Method) | - | - | 200-75 | 5 | 1200-700 | 1 | 10 |
| X108AD (1% Method) | - | - | 200-75 | 5 | 1200-700 | 1 | 10 |
| 161A1 GLASS BULK GROUNDMASS (Using all 5 analyses) | - | - | 0-0 | 5 | 1200-700 | 1 | 10 |
| X161AC GLASS BETWEEN MICROLITES (1% Method) | 54 | 1001 | 0-0 | 5 | 1200-700 | 1 | 10 |
| X108BC GLASS BETWEEN MICROLITES (Ranked Method) | - | - | 0-0 | 5 | 1200-700 | 1 | 10 |
| X108BC GLASS BETWEEN MICROLITES (1% Method) | - | - | 0-0 | 5 | 1200-700 | 1 | 10 |
| 109AC COARSELY VESICULAR GLASS (Ranked Method) | 105 | 887 | 0-0 | 5 | 1200-700 | 1 | 10 |
| X161AC MATRIX SHARDS BULK (No limit) | - | - | 0-0 | 5 | 1200-700 | 1 | 10 |
| X161AC GLASS BETWEEN MICROLITES (Ranked Method) | 54 | 1001 | 0-0 | 5 | 1200-700 | 1 | 10 |
| 274-1 (Ranked Method) | - | - | 0-0 | 5 | 1200-700 | 1 | 10 |
| 274-1 (1% Method, then adding ranked values past 1%) | - | - | 0-0 | 5 | 1200-700 | 1 | 10 |
| 13-301-1 (Only 2 analyses that looked like suitable glass) | - | - | 0-0 | 5 | 1200-700 | 1 | 10 |
| 108AC GLASS SITE 2 (Ranked Method) | - | - | 0-0 | 5 | 1200-700 | 1 | 10 |
| 108AC GLASS SITE 2 (1% Method) | - | - | 400-25 | 25 | 1200-700 | 1 | 10 |
| 109AC GLASS BETWEEN MICROLITES IN MICROLITE RICH AREAS (Ranked Method, all 9 analyses) | - | - | 400-25 | 25 | 1200-700 | 1 | 10 |
| 109AC FINELY VESICULAR GLASS (Ranked Method) | - | - | 400-25 | 25 | 1200-700 | 1 | 10 |
| 108B1 GLASS BETWEEN MICROLITES (Ranked Method) | - | - | 400-25 | 25 | 1200-700 | 1 | 10 |
| 108AC GLASS BETWEEN MICROLITES SITE 1 (Ranked Method) | - | - | 400-25 | 25 | 1200-700 | 1 | 10 |
| 225D3 LESS VESICULAR GLASS (alternative values; excluded highest value as it is 0.76% higher than all others, then ranked) | - | - | 400-25 | 25 | 1200-700 | 1 | 10 |
| 225 PINK ASH LIGHT SEPARATE GLASS (Ranked Method) | - | - | 400-25 | 25 | 1200-700 | 1 | 10 |

| Sample | Composition | | | | | | | | | | | | | |
|---|---|---|---|---|---|---|---|---|---|---|---|---|---|---|
| | $SiO_2$ | $TiO2$ | $Al_2O_3$ | $Fe_2O_3$ | $Cr_2O_3$ | FeO | MnO | MgO | NiO | CoO | CaO | $Na_2O$ | K2O | H2O |
| 129A3 GLASS TYPE 1 (Ranked Method; Banded Sample) | 72.09 | 0.59 | 14.17 | 0.00 | 0.00 | 2.88 | 0.00 | 0.58 | 0.00 | 0.00 | 2.15 | 3.64 | 3.89 | 10.00 |
| X129AC (Ranked Method) | 72.06 | 0.62 | 13.92 | 0.00 | 0.00 | 2.82 | 0.00 | 0.60 | 0.00 | 0.00 | 2.26 | 3.71 | 4.00 | 10.00 |
| 129A5 (Ranked Method) (subsidiary clast type, from second magma type in mingled eruption) | 72.62 | 0.51 | 14.03 | 0.00 | 0.00 | 2.45 | 0.00 | 0.55 | 0.00 | 0.00 | 2.06 | 3.78 | 3.99 | 10.00 |
| 129A5 (1% Method) (subsidiary clast type, from second magma type in mingled eruption) | 72.54 | 0.54 | 14.01 | 0.00 | 0.00 | 2.51 | 0.00 | 0.53 | 0.00 | 0.00 | 2.06 | 3.80 | 4.00 | 10.00 |
| X262AD (Ranked Method) | 70.99 | 0.73 | 14.18 | 0.00 | 0.00 | 3.25 | 0.00 | 0.73 | 0.00 | 0.00 | 2.52 | 3.93 | 3.65 | 10.00 |
| X129AC (1% Method) | 71.91 | 0.61 | 13.97 | 0.00 | 0.00 | 2.89 | 0.00 | 0.62 | 0.00 | 0.00 | 2.31 | 3.71 | 3.98 | 10.00 |
| 225CE (Ranked Method) | 70.32 | 0.73 | 14.66 | 0.00 | 0.00 | 3.32 | 0.00 | 0.78 | 0.00 | 0.00 | 2.60 | 4.12 | 3.47 | 10.00 |
| 225CE (1% Method) | 70.16 | 0.72 | 14.61 | 0.00 | 0.00 | 3.42 | 0.00 | 0.82 | 0.00 | 0.00 | 2.71 | 4.12 | 3.45 | 10.00 |
| 225DE (Ranked Method) | 70.10 | 0.78 | 14.61 | 0.00 | 0.00 | 3.39 | 0.00 | 0.84 | 0.00 | 0.00 | 2.72 | 4.09 | 3.47 | 10.00 |
| 225D3 LESS VESICULAR GLASS (Ranked) | 68.04 | 0.93 | 15.18 | 0.00 | 0.00 | 4.51 | 0.00 | 0.84 | 0.00 | 0.00 | 3.64 | 3.85 | 3.03 | 10.00 |
| 225D3 LESS VESICULAR GLASS Highest excluded | 68.04 | 0.93 | 15.18 | 0.00 | 0.00 | 4.51 | 0.00 | 0.84 | 0.00 | 0.00 | 3.64 | 3.85 | 3.03 | 10.00 |
| 225DE (1% Method) | 69.92 | 0.75 | 14.71 | 0.00 | 0.00 | 3.41 | 0.00 | 0.86 | 0.00 | 0.00 | 2.83 | 4.06 | 3.45 | 10.00 |
| 225-5B (Ranked Method) | 70.09 | 0.74 | 14.66 | 0.00 | 0.00 | 3.32 | 0.00 | 0.84 | 0.00 | 0.00 | 2.69 | 4.25 | 3.41 | 10.00 |
| 225B1 (1% Method) | 69.43 | 0.82 | 14.87 | 0.00 | 0.00 | 3.68 | 0.00 | 0.90 | 0.00 | 0.00 | 3.10 | 3.83 | 3.38 | 10.00 |
| 262-Y1 (1% Method) | 70.45 | 0.74 | 14.38 | 0.00 | 0.00 | 3.43 | 0.00 | 0.82 | 0.00 | 0.00 | 2.68 | 4.11 | 3.41 | 10.00 |
| X262AD (1% Method) | 70.84 | 0.75 | 14.24 | 0.00 | 0.00 | 3.33 | 0.00 | 0.73 | 0.00 | 0.00 | 2.51 | 3.94 | 3.67 | 10.00 |
| 225AC (1% Method) | 69.32 | 0.80 | 14.78 | 0.00 | 0.00 | 3.75 | 0.00 | 0.96 | 0.00 | 0.00 | 3.02 | 4.04 | 3.33 | 10.00 |
| 225A1 (1% Method) | 69.48 | 0.81 | 14.62 | 0.00 | 0.00 | 3.94 | 0.00 | 0.78 | 0.00 | 0.00 | 2.98 | 3.87 | 3.52 | 10.00 |
| 225AC (Ranked Method) | 69.51 | 0.82 | 14.78 | 0.00 | 0.00 | 3.64 | 0.00 | 0.94 | 0.00 | 0.00 | 2.98 | 3.99 | 3.34 | 10.00 |
| 225A1 (Ranked Method) | 69.60 | 0.83 | 14.51 | 0.00 | 0.00 | 3.99 | 0.00 | 0.77 | 0.00 | 0.00 | 2.90 | 3.86 | 3.54 | 10.00 |
| 225-5B (1% Method) | 69.94 | 0.75 | 14.65 | 0.00 | 0.00 | 3.42 | 0.00 | 0.86 | 0.00 | 0.00 | 2.72 | 4.22 | 3.44 | 10.00 |
| 225D1 Highest excluded | 69.54 | 0.75 | 14.84 | 0.00 | 0.00 | 3.59 | 0.00 | 0.92 | 0.00 | 0.00 | 3.08 | 3.90 | 3.39 | 10.00 |
| 225C1 (1% Method) | 69.07 | 0.82 | 14.96 | 0.00 | 0.00 | 3.71 | 0.00 | 1.02 | 0.00 | 0.00 | 2.99 | 4.17 | 3.26 | 10.00 |
| 262-Y1 (Ranked Method) | 70.45 | 0.76 | 14.40 | 0.00 | 0.00 | 3.40 | 0.00 | 0.83 | 0.00 | 0.00 | 2.71 | 4.07 | 3.39 | 10.00 |

| Sample | | | | | | | | | | | | | | |
|---|---|---|---|---|---|---|---|---|---|---|---|---|---|---|
| 13-107 (Ranked Method) | 69.68 | 0.73 | 14.67 | 0.00 | 0.00 | 3.61 | 0.00 | 0.99 | 0.00 | 0.00 | 2.96 | 4.00 | 3.37 | 10.00 |
| 13-107 (1% Method) | 69.62 | 0.74 | 14.70 | 0.00 | 0.00 | 3.61 | 0.00 | 0.99 | 0.00 | 0.00 | 2.96 | 4.01 | 3.37 | 10.00 |
| 225D3 MORE VESICULAR GLASS (Ranked Method) | 69.74 | 0.77 | 14.65 | 0.00 | 0.00 | 3.72 | 0.00 | 0.89 | 0.00 | 0.00 | 2.84 | 3.70 | 3.70 | 10.00 |
| 259-1-2 MATRIX GLASS (Ranked Method) | 72.05 | 0.64 | 14.06 | 0.00 | 0.00 | 2.51 | 0.00 | 0.73 | 0.00 | 0.00 | 2.22 | 3.67 | 4.11 | 10.00 |
| 259-1-2 CLAST INTERIOR (Ranked Method) | 69.89 | 0.72 | 14.85 | 0.00 | 0.00 | 3.44 | 0.00 | 0.86 | 0.00 | 0.00 | 3.45 | 3.46 | 3.34 | 10.00 |
| 12-225-19A (Ranked Method) | 68.75 | 0.94 | 14.21 | 0.00 | 0.00 | 4.91 | 0.00 | 0.96 | 0.00 | 0.00 | 3.25 | 3.76 | 3.23 | 10.00 |
| 225B1 (Ranked Method) | 69.73 | 0.80 | 14.67 | 0.00 | 0.00 | 3.53 | 0.00 | 0.92 | 0.00 | 0.00 | 3.03 | 3.89 | 3.45 | 10.00 |
| 13-262-4 GLASS TYPE 2 (RHS) (other alternative method) | 66.57 | 0.97 | 15.52 | 0.00 | 0.00 | 4.83 | 0.00 | 1.49 | 0.00 | 0.00 | 3.71 | 4.01 | 2.91 | 10.00 |
| 259-1-2 GLASS CHILLED MARGIN (Ranked Method) | 70.37 | 0.75 | 14.36 | 0.00 | 0.00 | 3.46 | 0.00 | 0.94 | 0.00 | 0.00 | 2.69 | 3.50 | 3.95 | 10.00 |
| 12-225-19A BULK (All 5 analyses) | 63.07 | 0.65 | 18.29 | 0.00 | 0.00 | 4.45 | 0.00 | 1.36 | 0.00 | 0.00 | 6.24 | 3.92 | 2.02 | 10.00 |
| 225C1 (Ranked Method) | 69.32 | 0.79 | 14.89 | 0.00 | 0.00 | 3.68 | 0.00 | 1.03 | 0.00 | 0.00 | 2.93 | 4.10 | 3.25 | 10.00 |
| RING PLAIN M1 LIGHT SEPARATE (Ranked Method) | 67.93 | 0.87 | 14.95 | 0.00 | 0.00 | 4.71 | 0.00 | 1.00 | 0.00 | 0.00 | 3.99 | 3.55 | 2.99 | 10.00 |
| 225D3 MORE VESICULAR BULK (All 3 Analyses) | 67.85 | 0.75 | 15.33 | 0.00 | 0.00 | 4.24 | 0.00 | 1.15 | 0.00 | 0.00 | 3.88 | 4.00 | 2.79 | 10.00 |
| 13-262-4 GLASS TYPE 2 (RHS) (Ranked Method) | 66.57 | 0.97 | 15.52 | 0.00 | 0.00 | 4.83 | 0.00 | 1.49 | 0.00 | 0.00 | 3.71 | 4.01 | 2.91 | 10.00 |
| 13-262-4 GLASS TYPE 1 (LHS) (Ranked Method) | 66.31 | 0.91 | 15.41 | 0.00 | 0.00 | 4.72 | 0.00 | 1.43 | 0.00 | 0.00 | 3.69 | 3.63 | 3.91 | 10.00 |
| 13-262-4 GLASS TYPE 1 (LHS) (1% Method) | 66.24 | 0.90 | 15.43 | 0.00 | 0.00 | 4.76 | 0.00 | 1.45 | 0.00 | 0.00 | 3.70 | 3.63 | 3.89 | 10.00 |
| 225D1 (Ranked Method) | 69.49 | 0.75 | 14.78 | 0.00 | 0.00 | 3.54 | 0.00 | 0.95 | 0.00 | 0.00 | 3.08 | 4.00 | 3.42 | 10.00 |
| 129A3 GLASS TYPE 2 (Ranked Method, Banded Sample) | 69.68 | 0.80 | 14.45 | 0.00 | 0.00 | 4.16 | 0.00 | 0.78 | 0.00 | 0.00 | 2.93 | 3.64 | 3.55 | 10.00 |
| 129A3 GLASS TYPE 2 (1% Method, Banded Sample) | 69.51 | 0.77 | 14.70 | 0.00 | 0.00 | 4.12 | 0.00 | 0.79 | 0.00 | 0.00 | 3.00 | 3.64 | 3.48 | 10.00 |
| 12-225-19A (1% Method) | 68.69 | 0.92 | 14.22 | 0.00 | 0.00 | 4.89 | 0.00 | 1.00 | 0.00 | 0.00 | 3.33 | 3.69 | 3.27 | 10.00 |
| 108A1 GLASS BETWEEN MICROLITES (Ranked Method) | 64.08 | 1.12 | 15.09 | 0.00 | 0.00 | 6.91 | 0.00 | 1.74 | 0.00 | 0.00 | 4.82 | 3.50 | 2.73 | 10.00 |
| 108A1 GLASS BETWEEN MICROLITES (1% Method) | 63.85 | 1.11 | 15.15 | 0.00 | 0.00 | 7.01 | 0.00 | 1.74 | 0.00 | 0.00 | 5.04 | 3.49 | 2.63 | 10.00 |
| 108A1 BULK GROUNDMASS (All 5 analyses) | 61.18 | 0.92 | 17.11 | 0.00 | 0.00 | 6.31 | 0.00 | 2.49 | 0.00 | 0.00 | 6.41 | 3.53 | 2.05 | 10.00 |

| | | | | | | | | | | | | | |
|---|---|---|---|---|---|---|---|---|---|---|---|---|---|
| 161A1 GLASS BETWEEN MICROLITES (Ranked Method) | 63.01 | 1.07 | 15.71 | 0.00 | 0.00 | 6.85 | 0.00 | 2.17 | 0.00 | 0.00 | 5.26 | 3.56 | 2.37 | 10.00 |
| 109AC GLASS SITES 8-9 (Ranked Method, all 10 analyses) | 62.70 | 0.94 | 16.11 | 0.00 | 0.00 | 6.33 | 0.00 | 2.50 | 0.00 | 0.00 | 5.49 | 3.63 | 2.30 | 10.00 |
| X108AD (Ranked Method) | 64.88 | 1.00 | 15.01 | 0.00 | 0.00 | 6.25 | 0.00 | 1.88 | 0.00 | 0.00 | 4.56 | 3.68 | 2.74 | 10.00 |
| X108AD (1% Method) | 64.67 | 0.95 | 15.41 | 0.00 | 0.00 | 6.04 | 0.00 | 1.92 | 0.00 | 0.00 | 4.59 | 3.70 | 2.71 | 10.00 |
| 161A1 GLASS BULK GROUNDMASS (Using all 5 analyses) | 60.77 | 0.95 | 17.26 | 0.00 | 0.00 | 6.24 | 0.00 | 2.77 | 0.00 | 0.00 | 6.51 | 3.56 | 1.93 | 10.00 |
| X161AC GLASS BETWEEN MICROLITES (1% Method) | 63.59 | 1.13 | 15.69 | 0.00 | 0.00 | 6.77 | 0.00 | 1.68 | 0.00 | 0.00 | 5.06 | 3.43 | 2.66 | 10.00 |
| X108BC GLASS BETWEEN MICROLITES (Ranked Method) | 64.87 | 1.15 | 14.67 | 0.00 | 0.00 | 6.87 | 0.00 | 1.60 | 0.00 | 0.00 | 4.39 | 3.63 | 2.82 | 10.00 |
| X108BC GLASS BETWEEN MICROLITES (1% Method) | 64.81 | 1.16 | 14.64 | 0.00 | 0.00 | 6.89 | 0.00 | 1.62 | 0.00 | 0.00 | 4.45 | 3.64 | 2.80 | 10.00 |
| 109AC COARSELY VESICULAR GLASS (Ranked Method) | 70.50 | 0.77 | 14.09 | 0.00 | 0.00 | 3.73 | 0.00 | 0.85 | 0.00 | 0.00 | 2.75 | 3.66 | 3.67 | 10.00 |
| X161AC MATRIX SHARDS BULK (No limit) | 61.43 | 0.91 | 17.44 | 0.00 | 0.00 | 5.88 | 0.00 | 2.38 | 0.00 | 0.00 | 6.37 | 3.50 | 2.09 | 10.00 |
| X161AC GLASS BETWEEN MICROLITES (Ranked Method) | 63.59 | 1.13 | 15.69 | 0.00 | 0.00 | 6.77 | 0.00 | 1.68 | 0.00 | 0.00 | 5.06 | 3.43 | 2.66 | 10.00 |
| 274-1 (Ranked Method) | 70.20 | 0.63 | 15.10 | 0.00 | 0.00 | 3.15 | 0.00 | 0.74 | 0.00 | 0.00 | 3.01 | 3.94 | 3.24 | 10.00 |
| 274-1 (1% Method, then adding ranked values past 1%) | 70.20 | 0.63 | 15.10 | 0.00 | 0.00 | 3.15 | 0.00 | 0.74 | 0.00 | 0.00 | 3.01 | 3.94 | 3.24 | 10.00 |
| 13-301-1 (Only 2 analyses that looked like suitable glass) | 60.84 | 0.26 | 20.66 | 0.00 | 0.00 | 2.59 | 0.00 | 0.83 | 0.00 | 0.00 | 4.78 | 4.13 | 5.93 | 10.00 |
| 108AC GLASS SITE 2 (Ranked Method) | 73.75 | 0.68 | 12.82 | 0.00 | 0.00 | 2.86 | 0.00 | 0.47 | 0.00 | 0.00 | 1.70 | 3.59 | 4.13 | 10.00 |
| 108AC GLASS SITE 2 (1% Method) | 73.63 | 0.67 | 12.88 | 0.00 | 0.00 | 2.84 | 0.00 | 0.49 | 0.00 | 0.00 | 1.73 | 3.66 | 4.11 | 10.00 |
| 109AC GLASS BETWEEN MICROLITES IN MICROLITE RICH AREAS (Ranked Method, all 9 analyses) | 63.63 | 1.15 | 15.17 | 0.00 | 0.00 | 7.55 | 0.00 | 1.56 | 0.00 | 0.00 | 4.97 | 3.48 | 2.51 | 10.00 |
| 109AC FINELY VESICULAR GLASS (Ranked Method) | 64.30 | 0.91 | 15.84 | 0.00 | 0.00 | 5.81 | 0.00 | 1.98 | 0.00 | 0.00 | 4.95 | 3.49 | 2.73 | 10.00 |
| 108B1 GLASS BETWEEN MICROLITES (Ranked Method) | 63.78 | 1.18 | 14.87 | 0.00 | 0.00 | 7.40 | 0.00 | 1.70 | 0.00 | 0.00 | 4.97 | 3.33 | 2.78 | 10.00 |
| 108AC GLASS BETWEEN MICROLITES SITE 1 (Ranked | 64.19 | 1.13 | 15.26 | 0.00 | 0.00 | 6.76 | 0.00 | 1.56 | 0.00 | 0.00 | 4.76 | 3.60 | 2.72 | 10.00 |

| | | | | | | | | | | | | | | |
|---|---|---|---|---|---|---|---|---|---|---|---|---|---|---|
| Method) | | | | | | | | | | | | | | |
| 225D3 LESS VESICULAR GLASS (alternative values; excluded highest value as it is 0.76% higher than all others, then ranked) | 68.04 | 0.93 | 15.18 | 0.00 | 0.00 | 4.51 | 0.00 | 0.84 | 0.00 | 0.00 | 3.64 | 3.85 | 3.03 | 10.00 |
| 225 PINK ASH LIGHT SEPARATE GLASS (Ranked Method) | 69.42 | 0.82 | 15.09 | 0.00 | 0.00 | 3.67 | 0.00 | 0.96 | 0.00 | 0.00 | 2.86 | 4.00 | 3.19 | 10.00 |

**Table 3.** Mt Ruapehu magma-meter results (top) and compositions (bottom). If the magma-meter was not able to calculate a triple-junction, there is a "-" symbol. The $f_{O2}$ and $H_2O$ ranges represent those which were closest to producing a triple-junction, although most compositions were tested from 0 - +2 $\Delta$QFM.

range from 100 to 148 MPa (3.9 – 5.8 km), and there are two distinct modes at ~110 MPa and

~130 MPa for the ranked method data, Figure 6. Although the 1% method gives similar pressure

calculations, the perceived bimodal pressure distribution disappears when considering the results

from the 1% method, Figure 6. However, the range from 100 to 148 MPa is consistent between

ranked and 1% methods.
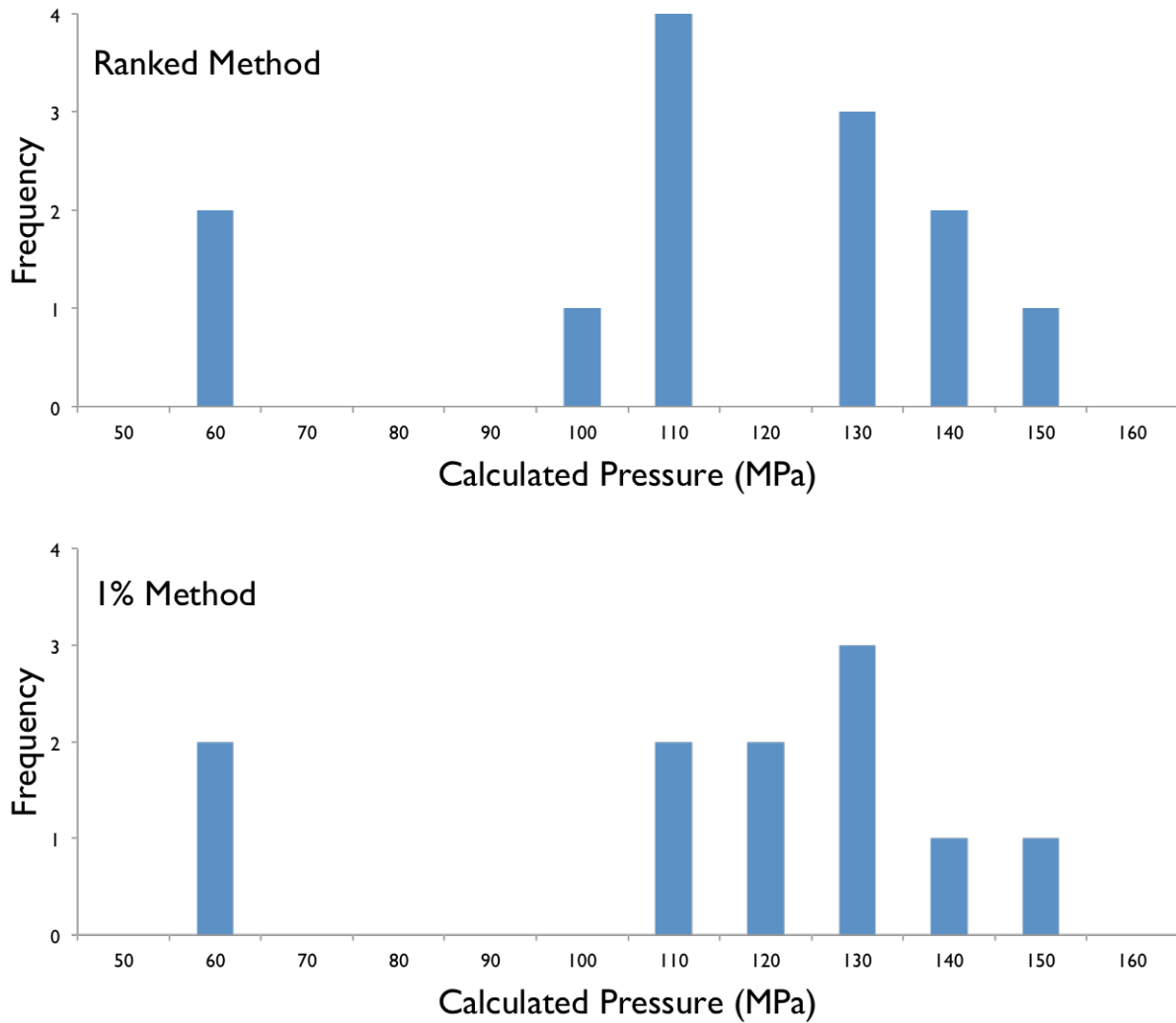


**Figure 6.** Frequency of calculated pressures using glass compositions calculated using the ranked method (top panel) and 1% method (bottom panel) for Mt Ruapehu. The distribution of pressures is similar for the two glass averaging methods. The calculated pressures range from 54 MPa to 148 MPa, with the majority of the calculations in the 100-150 MPa range.

*Implications for Mt Ruapehu Evolution:*

It is interesting to combine the results from the magma-meter with the volcanological evidence

gathered by James Cowlyn (2016) to understand the evolution of storage conditions for magmas

that fed Ruapehu PDCs.
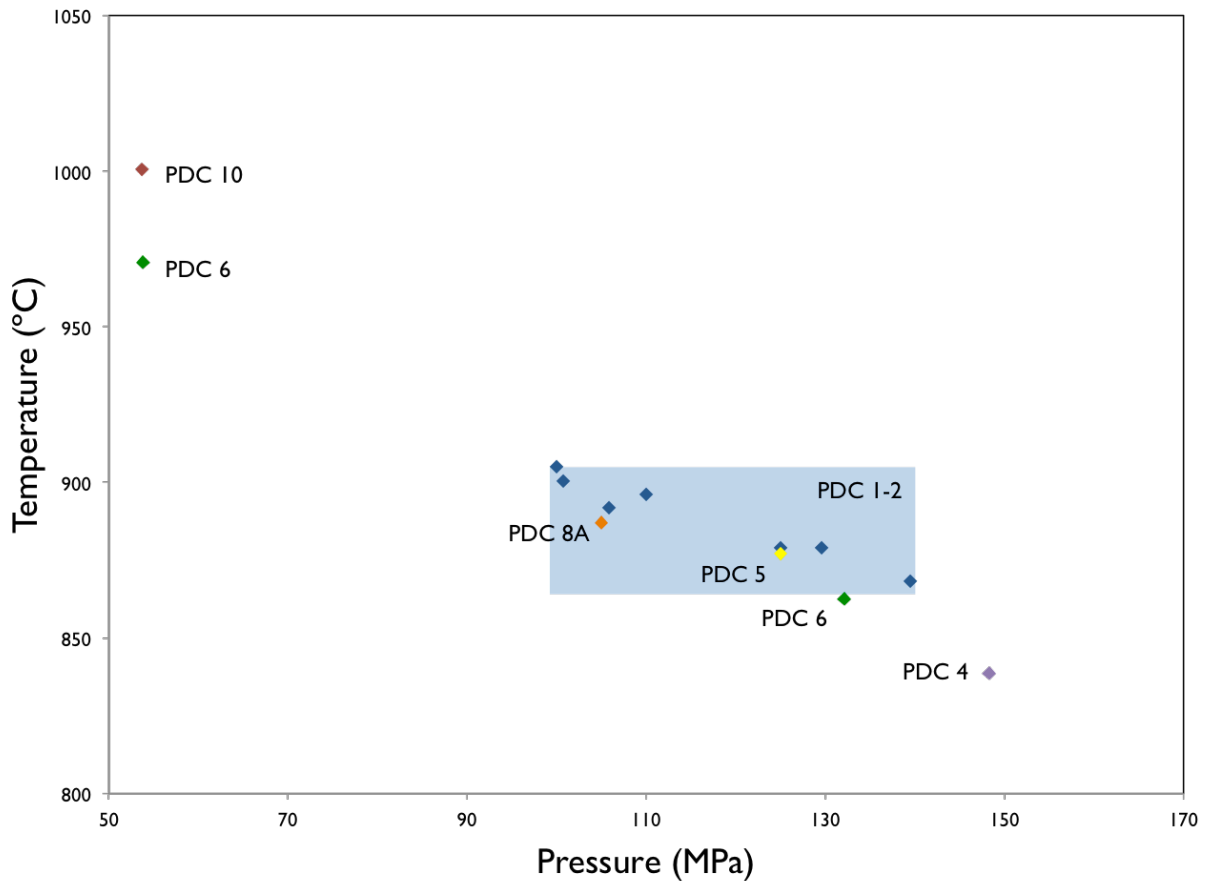


**Figure 7.** Mt Ruapehu pressure-temperature results using the ranked method magma-meter calculations. The temperature range of the samples is 1000-840 ºC , and the pressure range is 54-148 MPa. The blue data points in the blue box are from PDC 1 and PDC 2; all other data points are labeled with PDC eruption. When correlated to the PDC units, storage conditions through time emerge. The older PDC units are cooler and deeper, while the younger PDC units are hotter and shallower. The progression is evidenced by the eruptive style and vents at Mt Ruapehu, Figure 5.

The distribution of pressures and temperatures calculated using the magma-meter directly correlates not only with the ages of eruptions, but also with the styles of eruption and vent configuration at Mt Ruapehu, Figure 7. As discussed above, vents and styles of pyroclastic eruptions at Mt Ruapehu changed over time, with older magmas erupting from the North Crater, and younger magmas erupting from vents located in the South Crater while transitioning to a characteristically less explosive eruption style, Figure 5.

The storage conditions of the oldest units are relatively deep and cool, while the younger, smaller and denser PDCs are both shallower and hotter.   The difference in pressure and eruptive style corresponds to the change in eruptive vents, indicating that magmas erupted earlier from the North Crater are sourced from a deeper and hotter magma body than those erupted from the South Crater.  Using the magma-meter, we can not only determine pre-eruptive storage conditions, but also show that there was a change in storage pressure, indicating two distinct storage depths through Mt Ruapehu's history. We cannot at this point determine whether this difference corresponds to two separate magma batches that are tapped and give rise to contrasting eruptions, or whether it indicates that different portions of a larger magma body are being tapped at different times.

**Application to Natural Systems – Paraná Palmas Unit:**

The magma-meter was also applied to the Palmas unit of the Paraná large igneous province (LIP), Brazil. The basalts of the Serra Geral formation that fill the Paraná Basin are a part of an LIP associated with the rifting of the South Atlantic Ocean from 140-135 Ma (Hawkesworth et al, 2000). The Paraná LIP is predominantly basaltic with a large stack of silicic units capping the

| Sample | Magma-Meter Results | | Magma-Meter Parameters | | | | | |
|---|---|---|---|---|---|---|---|---|
| | P (MPa) | T (ºC) | P Range (MPa) | P step (MPa) | T Range (ºC) | fO2 (ΔQFM) | H2O (wt %) |
| PEV26H_2.1_Spectrum 805 | - | - | 400-50 | 50 | 1200-700 | 1 | 10 |
| PEV26H_2.11_Spectrum 854 | - | - | 450-50 | 50 | 1200-700 | 1 | 10 |
| PEV26H_2.11_Spectrum 857 | - | - | 450-50 | 50 | 1200-700 | 1 | 10 |
| PEV26H_2.12_Spectrum 863 | - | - | 450-50 | 50 | 1200-700 | 0 - +2 | 10 |
| PEV26H_2.12_Spectrum 864 | - | - | 400-50 | 50 | 1200-700 | 0 - +2 | 10-2 |
| PEV26H_2.15_Spectrum 874 | - | - | 450-50 | 50 | 1200-700 | 1 | 10 |
| PEV26H_2.15_Spectrum 875 | - | - | 400-50 | 50 | 1200-700 | 1 | 10 |
| PEV26H_2.16_Spectrum 876 | - | - | 450-450 | 50 | 1200-700 | 1 | 10 |
| PEV26H_2.16_Spectrum 879 | - | - | 450-50 | 50 | 1200-700 | 1 | 10 |
| PEV26H_2.2_Spectrum 807 | - | - | 450-50 | 50 | 1200-700 | 1 | 10 |
| PEV26H_2.2_Spectrum 811 | - | - | 450-50 | 50 | 1200-700 | 1 | 10 |
| PEV26H_2.4_Spectrum 823 | - | - | 450-50 | 50 | 1200-700 | 1 | 10 |
| PEV26H_2.6_Spectrum 841 | - | - | 400-50 | 50 | 1200-700 | 0 - +2 | 10 |
| PEV26H_2.9_Spectrum 846 | - | - | 400-50 | 50 | 1200-700 | 1 | 10 |
| PEV26J_1.1_Spectrum 1072 | - | - | 400-50 | 50 | 1200-700 | 1 | 10 |
| PEV26J_1.1_Spectrum 1073 | - | - | 400-50 | 50 | 1200-700 | 1 | 10 |
| PEV26J_1.1_Spectrum 1074 | - | - | 400-50 | 50 | 1200-700 | 1 | 10 |
| PEV26J_1.10_Spectrum 1144 | - | - | 400-50 | 50 | 1200-700 | 1 | 10 |
| PEV26J_1.10_Spectrum 1151 | - | - | 400-50 | 50 | 1200-700 | 1 | 10 |
| PEV26J_1.10_Spectrum 1153 | - | - | 400-50 | 50 | 1200-700 | 1 | 10 |
| PEV26J_1.11_Spectrum 1160 | - | - | 400-50 | 50 | 1200-700 | 1 | 10 |
| PEV26J_1.11_Spectrum 1161 | - | - | 400-50 | 50 | 1200-700 | 1 | 10 |
| PEV26J_1.11_Spectrum 1162 | - | - | 400-50 | 50 | 1200-700 | 1 | 10 |
| PEV26J_1.12_Spectrum 1176 | - | - | 400-50 | 50 | 1200-700 | 1 | 10 |
| PEV26J_1.13_Spectrum 1179 | - | - | 400-50 | 50 | 1200-700 | 1 | 10 |
| PEV26J_1.13_Spectrum 1180 | - | - | 400-50 | 50 | 1200-700 | 1 | 10 |
| PEV26J_1.13_Spectrum 1181 | - | - | 400-50 | 50 | 1200-700 | 1 | 10 |
| PEV26J_1.13_Spectrum 1182 | - | - | 400-50 | 50 | 1200-700 | 1 | 10 |

| | | | | | | | |
|---|---|---|---|---|---|---|---|
| PEV26J_1.14_Spectrum 1185 | - | - | 400-50 | 50 | 1200-700 | 1 | 10 |
| PEV26J_1.14_Spectrum 1186 | - | - | 400-50 | 50 | 1200-700 | 1 | 10 |
| PEV26J_1.15_Spectrum 1189 | - | - | 400-50 | 50 | 1200-700 | 1 | 10 |
| PEV26J_1.15_Spectrum 1190 | - | - | 400-50 | 50 | 1200-700 | 1 | 10 |
| PEV26J_1.15_Spectrum 1192 | - | - | 400-50 | 50 | 1200-700 | 1 | 10 |
| PEV26J_1.15_Spectrum 1193 | - | - | 400-50 | 50 | 1200-700 | 1 | 10 |
| PEV26J_1.2_Spectrum 1080 | - | - | 400-50 | 50 | 1200-700 | 1 | 10 |
| PEV26J_1.3_Spectrum 1089 | - | - | 400-50 | 50 | 1200-700 | 1 | 10 |
| PEV26J_1.3_Spectrum 1090 | - | - | 300-25 | 5 | 1200-700 | 0 - +2 | 10-3 |
| PEV26J_1.6_Spectrum 1110 | - | - | 400-50 | 50 | 1200-700 | 1 | 10 |
| PEV26J_1.7_Spectrum 1115 | - | - | 400-50 | 50 | 1200-700 | 1 | 10 |
| PEV26J_1.7_Spectrum 1117 | - | - | 400-50 | 50 | 1200-700 | 1 | 10 |
| PEV26J_1.7_Spectrum 1118 | - | - | 400-50 | 50 | 1200-700 | 1 | 10 |
| PEV26J_1.7_Spectrum 1120 | - | - | 400-50 | 50 | 1200-700 | 1 | 10 |
| PEV26J_1.7_Spectrum 1125 | - | - | 400-50 | 50 | 1200-700 | 1 | 10 |
| PEV26J_1.8_Spectrum 1127 | - | - | 400-50 | 50 | 1200-700 | 1 | 10 |
| PEV26J_1.9_Spectrum 1135 | - | - | 400-50 | 50 | 1200-700 | 1 | 10 |
| PEV26J_1.9_Spectrum 1136 | - | - | 400-50 | 50 | 1200-700 | 1 | 10 |
| PEV26K_1_11_Spectrum_1409 | - | - | 400-25 | 5 | 1200-700 | 1 | 10 |
| PEV26K_1_12_Spectrum_1416 | - | - | 400-25 | 5 | 1200-700 | 1 | 10 |
| PEV26K_1_13_Spectrum_1417 | - | - | 400-25 | 5 | 1200-700 | 1 | 10 |
| PEV26K_1_13_Spectrum_1418 | - | - | 400-25 | 5 | 1200-700 | 1 | 10 |
| PEV26K_1_14_Spectrum_1425 | - | - | 400-25 | 5 | 1200-700 | 1 | 10 |
| PEV26K_1_16_Spectrum_1433 | - | - | 400-25 | 5 | 1200-700 | 1 | 10 |
| PEV26K_1_2_Spectrum_1363 | - | - | 400-25 | 5 | 1200-700 | 1 | 10 |
| PEV26K_1_4_Spectrum_1371 | - | - | 400-25 | 5 | 1200-700 | 1 | 10 |
| PEV26K_1_6_Spectrum_1379 | - | - | 400-25 | 5 | 1200-700 | 1 | 10 |
| PEV26K_1_6_Spectrum_1381 | - | - | 400-25 | 25 | 1200-700 | 1 | 10 |
| PEV26K_1_7_Spectrum_1384 | - | - | 400-25 | 25 | 1200-700 | 1 | 10 |
| PEV26K_1_8_Spectrum_1395 | - | - | 400-25 | 25 | 1200-700 | 1 | 10 |
| pev26d1_1.1_1 | - | - | 400-50 | 50 | 1200-700 | 1 | 10 |

| | | | | | | | |
|---|---|---|---|---|---|---|---|
| pev26d1_1.1_2 | - | - | 400-50 | 50 | 1200-700 | 1 | 10 |
| pev26d1_1.1_4 | - | - | 400-50 | 25 | 1200-700 | 1 | 10 |
| pev26d1_1.1_7 | - | - | 300-25 | 25 | 1200-700 | 1 | 10 |
| pev26d1_1.2_1 | - | - | 300-50 | 50 | 1200-700 | 1 | 10 |
| pev26d1_1.2_2 | - | - | 300-50 | 50 | 1200-700 | 1 | 10 |
| pev26d1_1.2_3 | - | - | 300-50 | 25 | 1200-700 | 1 | 10 |
| pev26d1_1.2_4 | - | - | 300-50 | 25 | 1200-700 | 1 | 10 |
| pev26d1_1.2_5 | - | - | 300-50 | 25 | 1200-700 | 1 | 10 |
| pev26d1_1.2_6 | - | - | 300-50 | 25 | 1200-700 | 1 | 10 |
| pev26d1_1.2_7 | - | - | 300-50 | 25 | 1200-700 | 1 | 10 |
| pev26d1_1.4_3 | - | - | 300-50 | 50 | 1200-700 | 1 | 10 |
| pev26d1_1.6_1 | - | - | 300-50 | 50 | 1200-700 | 1 | 10 |
| pev26d1_1.6_2 | - | - | 300-50 | 50 | 1200-700 | 1 | 10 |
| pev26d1_1.6_3 | - | - | 300-50 | 25 | 1200-700 | 1 | 10 |
| pev26d1_1.6_5 | - | - | 300-50 | 50 | 1200-700 | 1 | 10 |
| pev26d1_1.6_6 | - | - | 300-50 | 50 | 1200-700 | 1 | 10 |
| pev26d1_1.6_7 | - | - | 300-50 | 50 | 1200-700 | 1 | 10 |
| pev26d1_1.6_8 | - | - | 300-50 | 50 | 1200-700 | 1 | 10 |
| pev26d1_1.8_1 | - | - | 300-50 | 50 | 1200-700 | 1 | 10 |
| pev26d1_1.8_2 | - | - | 300-50 | 50 | 1200-700 | 1 | 10 |
| pev26d1_1.8_3 | - | - | 300-50 | 50 | 1200-700 | 1 | 10 |
| pev26d1_1.9_1 | - | - | 300-50 | 50 | 1200-700 | 1 | 10 |
| pev26d1_1.9_2 | - | - | 300-50 | 50 | 1200-700 | 1 | 10 |
| pev26d1_1.9_3 | - | - | 300-50 | 50 | 1200-700 | 1 | 10 |
| pev26d1_1.9_4 | - | - | 300-50 | 50 | 1200-700 | 1 | 10 |
| pev26d1_1.9_5 | - | - | 300-50 | 50 | 1200-700 | 1 | 10 |
| pev26d1_1.9_6 | - | - | 300-50 | 50 | 1200-700 | 1 | 10 |
| pev26d1_1.9_7 | - | - | 300-50 | 50 | 1200-700 | 1 | 10 |
| pev26d1_1.10_1 | - | - | 300-50 | 50 | 1200-700 | 1 | 10 |
| pev26d1_1.10_2 | - | - | 300-50 | 50 | 1200-700 | 1 | 10 |
| pev26d1_1.11_2 | - | - | 300-50 | 50 | 1200-700 | 1 | 10 |

31

| | | | | | | | |
|---|---|---|---|---|---|---|---|
| pev26d1_1.11_3 | - | - | 300-50 | 50 | 1200-700 | 1 | 10 |
| pev26d1_1.11_4 | - | - | 300-50 | 50 | 1200-700 | 1 | 10 |
| pev26d1_1.11_5 | - | - | 300-50 | 50 | 1200-700 | 1 | 10 |
| pev26d1_1.11_6 | - | - | 300-50 | 50 | 1200-700 | 1 | 10 |
| pev26d1_1.11_7 | - | - | 300-50 | 50 | 1200-700 | 1 | 10 |
| pev26d1_1.12_1 | - | - | 300-25 | 50 | 1200-700 | 1 | 10 |
| pev26d1_1.12_2 | - | - | 300-25 | 50 | 1200-700 | 1 | 10 |
| pev26d1_1.12_3 | - | - | 300-25 | 50 | 1200-700 | 1 | 10 |
| pev26d1_1.12_4 | - | - | 300-25 | 50 | 1200-700 | 1 | 10 |
| pev26d1_1.13_1 | - | - | 300-25 | 50 | 1200-700 | 1 | 10 |
| pev26d1_1.13_2 | - | - | 300-25 | 50 | 1200-700 | 1 | 10 |
| pev26d1_1.14_1 | 97 | 785 | 300-25 | 50 | 1200-700 | 1 | 10 |
| pev26d1_1.14_2 | - | - | 300-25 | 50 | 1200-700 | 1 | 10 |
| pev26d1_1.14_3 | - | - | 300-25 | 50 | 1200-700 | 1 | 10 |
| pev26d1_1.14_4 | - | - | 300-25 | 50 | 1200-700 | 1 | 10 |
| pev26d1_1.14_5 | - | - | 300-25 | 50 | 1200-700 | 1 | 10 |
| pev26d1_1.15_1 | - | - | 300-25 | 25 | 1200-700 | 1 | 10 |
| pev26d1_1.15_3 | - | - | 300-25 | 25 | 1200-700 | 1 | 10 |
| pev26d1_1.15_4 | - | - | 300-25 | 25 | 1200-700 | 1 | 10 |
| pev26d1_1.16_1 | - | - | 300-25 | 25 | 1200-700 | 1 | 10 |
| pev26d1_1.16_2 | - | - | 300-25 | 25 | 1200-700 | 1 | 10 |
| pev26d1_1.16_3 | - | - | 300-25 | 25 | 1200-700 | 1 | 10 |
| pev26d1_1.16_4 | - | - | 300-25 | 25 | 1200-700 | 1 | 10 |
| pev26d1_1.18_1 | - | - | 300-25 | 25 | 1200-700 | 1 | 10 |
| pev26d1_1.18_2 | - | - | 300-25 | 25 | 1200-700 | 1 | 10 |
| pev26d1_1.18_3 | - | - | 300-25 | 25 | 1200-700 | 1 | 10 |
| pev26d1_1.18_4 | - | - | 300-25 | 25 | 1200-700 | 1 | 10 |
| pev26d1_1.18_5 | - | - | 300-25 | 25 | 1200-700 | 1 | 10 |
| pev26d1_1.19_1 | - | - | 300-25 | 25 | 1200-700 | 1 | 10 |
| pev26d1_1.19_2 | - | - | 300-25 | 25 | 1200-700 | 1 | 10 |
| pev26d1_1.19_3 | - | - | 300-25 | 25 | 1200-700 | 1 | 10 |

| | | | | | | | |
|---|---|---|---|---|---|---|---|
| pev26d1_1.19_4 | - | - | 300-25 | 25 | 1200-700 | 1 | 10 |
| pev26d1_1.19_5 | - | - | 300-25 | 25 | 1200-700 | 1 | 10 |
| pev26d1_1.20_1 | - | - | 300-25 | 25 | 1200-700 | 1 | 10 |
| pev26d1_1.20_2 | - | - | 300-25 | 25 | 1200-700 | 1 | 10 |
| pev26d1_1.20_3 | - | - | 300-25 | 25 | 1200-700 | 1 | 10 |
| pev26d1_1.20_4 | - | - | 300-25 | 25 | 1200-700 | 1 | 10 |
| pev26d1_1.20_5 | - | - | 300-25 | 25 | 1200-700 | 1 | 10 |
| pev26d1_1.20_6 | - | - | 300-25 | 25 | 1200-700 | 1 | 10 |
| pev26d1_1.21_1 | - | - | 300-25 | 25 | 1200-700 | 1 | 10 |
| pev26d1_1.21_2 | - | - | 300-25 | 25 | 1200-700 | 1 | 10 |
| pev26d1_1.21_3 | - | - | 300-25 | 25 | 1200-700 | 1 | 10 |
| pev26d1_1.21_4 | - | - | 400-25 | 25 | 1200-700 | 1 | 10 |
| pev26d1_1.22_1 | - | - | 400-25 | 25 | 1200-700 | 1 | 10 |
| pev26d1_1.22_2 | - | - | 400-25 | 25 | 1200-700 | 1 | 10 |
| pev26d1_1.22_3 | - | - | 0-0 | 25 | 1200-700 | 1 | 10 |
| pev26d1_1.22_4 | - | - | 200-25 | 25 | 1200-700 | 1 | 10 |
| pev26d1_1.22_5 | - | - | 200-25 | 25 | 1200-700 | 1 | 10 |
| pev26d1_1.22_6 | - | - | 200-25 | 25 | 1200-700 | 1 | 10 |
| pev26d1_1.22_7 | - | - | 200-25 | 25 | 1200-700 | 1 | 10 |
| pev26d1_1.23_1 | - | - | 200-25 | 25 | 1200-700 | 1 | 10 |
| pev26d1_1.23_2 | - | - | 400-25 | 25 | 1200-700 | 1 | 10 |
| pev26d1_1.23_3 | - | - | 400-25 | 25 | 1200-700 | +1 - +4 | 10 |
| PEV26G_2_2_13 | - | - | 400-50 | 25 | 1200-700 | 1 | 10 |
| PEV26G_2_5_5 | - | - | 0-0 | 25 | 1200-700 | +1 - +4 | 0-10 |
| PEV26I_1.1_2 | - | - | 300-25 | 5 | 1200-700 | 1 | 10 |
| PEV26I_1.1_4 | - | - | 300-25 | 5 | 1200-700 | 1 | 10 |
| PEV26I_1.2_1 | - | - | 300-25 | 5 | 1200-700 | 1 | 10 |
| PEV26I_1.2_2 | - | - | 300-25 | 5 | 1200-700 | 1 | 10 |
| PEV26I_1.2_3 | - | - | 300-25 | 25 | 1200-700 | 1 | 10 |
| PEV26I_1.2_4 | - | - | 300-25 | 25 | 1200-700 | 1 | 10 |
| PEV26I_1.2_5 | - | - | 300-25 | 25 | 1200-700 | 1 | 10 |

PEV26I_1.2_6 | - - | 300-25 | 25 | 1200-700 | 1 | 10

| Sample | Composition | | | | | | | | | | | | | |
| | SiO2 | TiO2 | Al2O3 | Fe2O3 | Cr2O3 | FeO | MnO | MgO | NiO | CoO | CaO | Na2O | K2O | H2O |
| PEV26H_2.1_Spectrum 805 | 63.64 | 0.62 | 14.24 | 0.00 | 0.00 | 6.50 | 0.00 | 5.17 | 0.00 | 0.00 | 1.59 | 2.93 | 5.30 | 10.00 |
| PEV26H_2.11_Spectrum 854 | 66.51 | 0.53 | 13.83 | 0.00 | 0.00 | 4.68 | 0.00 | 3.49 | 0.00 | 0.00 | 1.23 | 3.30 | 5.05 | 10.00 |
| PEV26H_2.11_Spectrum 857 | 73.54 | 0.57 | 12.70 | 0.00 | 0.00 | 2.36 | 0.00 | 0.93 | 0.00 | 0.00 | 0.76 | 2.97 | 5.81 | 10.00 |
| PEV26H_2.12_Spectrum 863 | 63.48 | 0.69 | 15.49 | 0.00 | 0.00 | 5.29 | 0.00 | 4.02 | 0.00 | 0.00 | 2.28 | 3.84 | 4.50 | 10.00 |
| PEV26H_2.12_Spectrum 864 | 63.53 | 0.68 | 16.36 | 0.00 | 0.00 | 5.02 | 0.00 | 2.89 | 0.00 | 0.00 | 2.76 | 4.08 | 4.33 | 10.00 |
| PEV26H_2.15_Spectrum 874 | 68.13 | 0.82 | 13.49 | 0.00 | 0.00 | 3.92 | 0.00 | 3.63 | 0.00 | 0.00 | 0.95 | 2.57 | 6.49 | 10.00 |
| PEV26H_2.15_Spectrum 875 | 63.31 | 0.51 | 15.01 | 0.00 | 0.00 | 4.76 | 0.00 | 6.05 | 0.00 | 0.00 | 1.05 | 3.02 | 6.29 | 10.00 |
| PEV26H_2.16_Spectrum 876 | 64.53 | 0.60 | 15.68 | 0.00 | 0.00 | 3.84 | 0.00 | 5.18 | 0.00 | 0.00 | 1.54 | 4.22 | 3.94 | 10.00 |
| PEV26H_2.16_Spectrum 879 | 63.92 | 0.60 | 14.53 | 0.00 | 0.00 | 4.86 | 0.00 | 5.34 | 0.00 | 0.00 | 1.01 | 3.13 | 5.11 | 10.00 |
| PEV26H_2.2_Spectrum 807 | 67.22 | 0.56 | 13.57 | 0.00 | 0.00 | 5.42 | 0.00 | 2.54 | 0.00 | 0.00 | 1.10 | 2.85 | 5.98 | 10.00 |
| PEV26H_2.2_Spectrum 811 | 60.23 | 0.72 | 15.55 | 0.00 | 0.00 | 7.57 | 0.00 | 4.05 | 0.00 | 0.00 | 1.41 | 3.16 | 6.58 | 10.00 |
| PEV26H_2.4_Spectrum 823 | 62.47 | 0.62 | 15.19 | 0.00 | 0.00 | 6.16 | 0.00 | 4.46 | 0.00 | 0.00 | 1.31 | 3.54 | 5.60 | 10.00 |
| PEV26H_2.6_Spectrum 841 | 63.75 | 0.57 | 14.78 | 0.00 | 0.00 | 5.72 | 0.00 | 4.78 | 0.00 | 0.00 | 1.53 | 3.80 | 4.29 | 10.00 |
| PEV26H_2.9_Spectrum 846 | 63.38 | 0.46 | 15.51 | 0.00 | 0.00 | 5.56 | 0.00 | 4.25 | 0.00 | 0.00 | 1.33 | 3.32 | 5.71 | 10.00 |
| PEV26J_1.1_Spectrum 1072 | 63.07 | 0.97 | 17.37 | 0.00 | 0.00 | 4.46 | 0.00 | 2.22 | 0.00 | 0.00 | 1.29 | 4.42 | 6.20 | 10.00 |
| PEV26J_1.1_Spectrum 1073 | 63.36 | 0.93 | 17.37 | 0.00 | 0.00 | 4.19 | 0.00 | 2.22 | 0.00 | 0.00 | 1.01 | 3.98 | 6.94 | 10.00 |
| PEV26J_1.1_Spectrum 1074 | 63.88 | 0.80 | 17.06 | 0.00 | 0.00 | 4.62 | 0.00 | 2.19 | 0.00 | 0.00 | 1.27 | 4.25 | 5.93 | 10.00 |
| PEV26J_1.10_Spectrum 1144 | 61.99 | 0.93 | 16.92 | 0.00 | 0.00 | 5.63 | 0.00 | 3.39 | 0.00 | 0.00 | 1.50 | 4.26 | 5.38 | 10.00 |
| PEV26J_1.10_Spectrum 1151 | 62.29 | 0.95 | 17.14 | 0.00 | 0.00 | 5.18 | 0.00 | 2.91 | 0.00 | 0.00 | 1.26 | 4.34 | 5.92 | 10.00 |
| PEV26J_1.10_Spectrum 1153 | 64.11 | 0.78 | 16.38 | 0.00 | 0.00 | 4.72 | 0.00 | 2.42 | 0.00 | 0.00 | 1.07 | 3.82 | 6.69 | 10.00 |
| PEV26J_1.11_Spectrum 1160 | 61.74 | 0.89 | 16.58 | 0.00 | 0.00 | 5.96 | 0.00 | 3.99 | 0.00 | 0.00 | 1.29 | 3.74 | 5.81 | 10.00 |
| PEV26J_1.11_Spectrum 1161 | 63.16 | 0.65 | 15.53 | 0.00 | 0.00 | 5.28 | 0.00 | 3.86 | 0.00 | 0.00 | 2.09 | 3.40 | 5.25 | 10.00 |
| PEV26J_1.11_Spectrum 1162 | 63.56 | 0.84 | 15.77 | 0.00 | 0.00 | 5.54 | 0.00 | 3.33 | 0.00 | 0.00 | 1.13 | 3.29 | 6.54 | 10.00 |
| PEV26J_1.12_Spectrum 1176 | 68.20 | 0.69 | 14.50 | 0.00 | 0.00 | 3.99 | 0.00 | 1.85 | 0.00 | 0.00 | 0.84 | 2.71 | 7.23 | 10.00 |
| PEV26J_1.13_Spectrum 1179 | 63.77 | 0.88 | 17.73 | 0.00 | 0.00 | 4.26 | 0.00 | 1.62 | 0.00 | 0.00 | 1.35 | 4.98 | 5.41 | 10.00 |
| PEV26J_1.13_Spectrum 1180 | 63.98 | 0.98 | 17.08 | 0.00 | 0.00 | 4.25 | 0.16 | 1.28 | 0.00 | 0.00 | 1.04 | 3.92 | 7.30 | 10.00 |

| | | | | | | | | | | | | | | |
|---|---|---|---|---|---|---|---|---|---|---|---|---|---|---|
| PEV26J_1.13_Spectrum 1181 | 63.55 | 0.84 | 17.78 | 0.00 | 0.00 | 3.88 | 0.00 | 1.40 | 0.00 | 0.00 | 1.18 | 4.58 | 6.80 | 10.00 |
| PEV26J_1.13_Spectrum 1182 | 63.78 | 0.93 | 17.15 | 0.00 | 0.00 | 4.63 | 0.00 | 1.56 | 0.00 | 0.00 | 1.11 | 4.04 | 6.80 | 10.00 |
| PEV26J_1.14_Spectrum 1185 | 63.44 | 0.66 | 17.21 | 0.00 | 0.00 | 4.41 | 0.00 | 2.32 | 0.00 | 0.00 | 1.02 | 3.59 | 7.36 | 10.00 |
| PEV26J_1.14_Spectrum 1186 | 63.31 | 0.82 | 16.72 | 0.00 | 0.00 | 5.00 | 0.00 | 2.64 | 0.00 | 0.00 | 1.13 | 3.52 | 6.87 | 10.00 |
| PEV26J_1.15_Spectrum 1189 | 62.66 | 1.08 | 17.15 | 0.00 | 0.00 | 4.93 | 0.00 | 2.30 | 0.00 | 0.00 | 1.15 | 3.69 | 7.04 | 10.00 |
| PEV26J_1.15_Spectrum 1190 | 62.98 | 0.89 | 16.76 | 0.00 | 0.00 | 4.89 | 0.00 | 2.42 | 0.00 | 0.00 | 1.06 | 3.66 | 7.34 | 10.00 |
| PEV26J_1.15_Spectrum 1192 | 63.08 | 0.97 | 16.91 | 0.00 | 0.00 | 4.87 | 0.00 | 2.25 | 0.00 | 0.00 | 1.35 | 3.88 | 6.69 | 10.00 |
| PEV26J_1.15_Spectrum 1193 | 63.60 | 0.91 | 16.36 | 0.00 | 0.00 | 4.74 | 0.00 | 2.76 | 0.00 | 0.00 | 0.96 | 3.64 | 7.02 | 10.00 |
| PEV26J_1.2_Spectrum 1080 | 63.58 | 0.69 | 17.82 | 0.00 | 0.00 | 3.80 | 0.00 | 2.12 | 0.00 | 0.00 | 0.97 | 3.94 | 7.09 | 10.00 |
| PEV26J_1.3_Spectrum 1089 | 63.90 | 0.94 | 17.43 | 0.00 | 0.00 | 3.89 | 0.00 | 1.19 | 0.00 | 0.00 | 0.92 | 3.64 | 8.08 | 10.00 |
| PEV26J_1.3_Spectrum 1090 | 62.13 | 0.28 | 20.25 | 0.00 | 0.00 | 3.15 | 0.00 | 1.39 | 0.00 | 0.00 | 4.95 | 5.17 | 2.69 | 10.00 |
| PEV26J_1.6_Spectrum 1110 | 65.92 | 1.21 | 13.52 | 0.00 | 0.00 | 5.34 | 0.00 | 4.28 | 0.00 | 0.00 | 1.23 | 2.65 | 5.84 | 10.00 |
| PEV26J_1.7_Spectrum 1115 | 61.60 | 0.80 | 15.96 | 0.00 | 0.00 | 5.93 | 0.00 | 5.18 | 0.00 | 0.00 | 1.48 | 3.83 | 5.23 | 10.00 |
| PEV26J_1.7_Spectrum 1117 | 63.28 | 0.70 | 15.93 | 0.00 | 0.00 | 4.96 | 0.00 | 4.57 | 0.00 | 0.00 | 1.08 | 3.51 | 5.98 | 10.00 |
| PEV26J_1.7_Spectrum 1118 | 61.08 | 0.53 | 15.89 | 0.00 | 0.00 | 6.40 | 0.00 | 5.65 | 0.00 | 0.00 | 1.52 | 3.74 | 5.19 | 10.00 |
| PEV26J_1.7_Spectrum 1120 | 61.58 | 0.83 | 16.10 | 0.00 | 0.00 | 5.92 | 0.00 | 4.79 | 0.00 | 0.00 | 1.31 | 3.80 | 5.68 | 10.00 |
| PEV26J_1.7_Spectrum 1125 | 62.44 | 0.71 | 15.18 | 0.00 | 0.00 | 5.73 | 0.00 | 5.50 | 0.00 | 0.00 | 1.14 | 3.02 | 6.07 | 10.00 |
| PEV26J_1.8_Spectrum 1127 | 64.77 | 0.00 | 21.99 | 0.00 | 0.00 | 1.11 | 0.00 | 0.00 | 0.00 | 0.00 | 8.00 | 4.12 | 0.00 | 10.00 |
| PEV26J_1.9_Spectrum 1135 | 63.63 | 0.71 | 15.40 | 0.00 | 0.00 | 5.23 | 0.00 | 4.79 | 0.00 | 0.00 | 1.40 | 3.48 | 5.36 | 10.00 |
| PEV26J_1.9_Spectrum 1136 | 62.10 | 0.80 | 15.87 | 0.00 | 0.00 | 5.64 | 0.00 | 5.14 | 0.00 | 0.00 | 1.35 | 3.56 | 5.53 | 10.00 |
| PEV26K_1_11_Spectrum_1409 | 64.23 | 0.55 | 16.60 | 0.00 | 0.00 | 4.40 | 0.00 | 3.31 | 0.00 | 0.00 | 2.49 | 3.62 | 4.79 | 10.00 |
| PEV26K_1_12_Spectrum_1416 | 61.89 | 0.55 | 15.65 | 0.00 | 0.00 | 6.64 | 0.00 | 4.77 | 0.00 | 0.00 | 1.09 | 2.80 | 6.61 | 10.00 |
| PEV26K_1_13_Spectrum_1417 | 63.28 | 0.90 | 16.40 | 0.00 | 0.00 | 4.48 | 0.00 | 2.92 | 0.00 | 0.00 | 0.94 | 3.21 | 7.88 | 10.00 |
| PEV26K_1_13_Spectrum_1418 | 60.39 | 1.00 | 15.21 | 0.00 | 0.00 | 7.77 | 0.00 | 4.85 | 0.00 | 0.00 | 1.33 | 2.94 | 6.52 | 10.00 |
| PEV26K_1_14_Spectrum_1425 | 62.79 | 0.95 | 15.81 | 0 | 0 | 5.66 | 0 | 3.33 | 0 | 0 | 1.16 | 3.11 | 7.18 | 10 |
| PEV26K_1_16_Spectrum_1433 | 61.51 | 0.63 | 16.58 | 0 | 0 | 5.71 | 0 | 4.64 | 0 | 0 | 1.38 | 3.11 | 6.44 | 10 |
| PEV26K_1_2_Spectrum_1363 | 61.11 | 0.89 | 15.71 | 0.00 | 0.00 | 6.72 | 0.00 | 5.44 | 0.00 | 0.00 | 1.38 | 2.86 | 5.88 | 10.00 |
| PEV26K_1_4_Spectrum_1371 | 65.88 | 0.48 | 14.19 | 0.00 | 0.00 | 5.19 | 0.00 | 3.94 | 0.00 | 0.00 | 1.13 | 2.75 | 6.44 | 10.00 |
| PEV26K_1_6_Spectrum_1379 | 62.45 | 0.74 | 16.01 | 0.00 | 0.00 | 5.52 | 0.00 | 4.45 | 0.00 | 0.00 | 1.47 | 3.14 | 6.23 | 10.00 |
| PEV26K_1_6_Spectrum_1381 | 63.09 | 0.79 | 15.18 | 0.00 | 0.00 | 5.74 | 0.00 | 4.93 | 0.00 | 0.00 | 1.31 | 3.08 | 5.88 | 10.00 |
| PEV26K_1_7_Spectrum_1384 | 63.88 | 0.74 | 15.33 | 0.00 | 0.00 | 5.50 | 0.00 | 4.91 | 0.00 | 0.00 | 1.68 | 3.90 | 4.06 | 10.00 |

| | | | | | | | | | | | | | | |
|---|---|---|---|---|---|---|---|---|---|---|---|---|---|---|
| PEV26K_1_8_Spectrum_1395 | 72.35 | 0.71 | 12.11 | 0.00 | 0.00 | 4.10 | 0.20 | 1.01 | 0.00 | 0.00 | 2.87 | 2.92 | 3.74 | 10.00 |
| pev26d1_1.1_1 | 79.65 | 0.59 | 10.53 | 0.75 | 0 | 0 | 0 | 0 | 0 | 0 | 0.52 | 2.39 | 5.57 | 10 |
| pev26d1_1.1_2 | 78.02 | 0.3 | 11.76 | 0.63 | 0 | 0 | 0 | 0 | 0 | 0 | 0.3 | 2.56 | 6.44 | 10 |
| pev26d1_1.1_4 | 79.72 | 0.52 | 10.94 | 0.59 | 0 | 0 | 0 | 0 | 0 | 0 | 0.36 | 2.44 | 5.44 | 10 |
| pev26d1_1.1_7 | 79.76 | 0.57 | 10.65 | 0.62 | 0 | 0 | 0 | 0 | 0 | 0 | 0.3 | 2.49 | 5.59 | 10 |
| pev26d1_1.2_1 | 83.86 | 0.29 | 8.72 | 0.46 | 0 | 0 | 0 | 0 | 0 | 0 | 0.23 | 1.97 | 4.45 | 10 |
| pev26d1_1.2_2 | 79.82 | 0.47 | 10.8 | 0.7 | 0 | 0 | 0 | 0 | 0 | 0 | 0.44 | 2.51 | 5.26 | 10 |
| pev26d1_1.2_3 | 80.24 | 0.42 | 10.68 | 0.46 | 0 | 0 | 0 | 0 | 0 | 0 | 0.41 | 2.57 | 5.23 | 10 |
| pev26d1_1.2_4 | 80.22 | 0.36 | 10.89 | 0.31 | 0 | 0 | 0 | 0 | 0 | 0 | 0.36 | 2.47 | 5.38 | 10 |
| pev26d1_1.2_5 | 79.41 | 0.21 | 11.09 | 0.62 | 0 | 0 | 0 | 0 | 0 | 0 | 0.33 | 2.46 | 5.87 | 10 |
| pev26d1_1.2_6 | 79.21 | 0.63 | 10.49 | 1.56 | 0 | 0 | 0 | 0 | 0 | 0 | 0.45 | 2.59 | 5.08 | 10 |
| pev26d1_1.2_7 | 78.89 | 0.39 | 11.33 | 0.62 | 0 | 0 | 0 | 0 | 0 | 0 | 0.31 | 2.45 | 6.01 | 10 |
| pev26d1_1.4_3 | 79.48 | 0.53 | 10.65 | 0.75 | 0 | 0 | 0 | 0.11 | 0 | 0 | 0.48 | 2.53 | 5.47 | 10 |
| pev26d1_1.6_1 | 78.15 | 0.52 | 11.46 | 0.86 | 0 | 0 | 0 | 0 | 0 | 0 | 0.27 | 2.58 | 6.16 | 10 |
| pev26d1_1.6_2 | 77.49 | 0.54 | 11.79 | 1.01 | 0 | 0 | 0 | 0 | 0 | 0 | 0.4 | 2.64 | 6.13 | 10 |
| pev26d1_1.6_3 | 78.04 | 0.59 | 11.28 | 1.23 | 0 | 0 | 0 | 0 | 0 | 0 | 0.34 | 2.51 | 6 | 10 |
| pev26d1_1.6_5 | 80.74 | 0.41 | 10.48 | 0.29 | 0 | 0 | 0 | 0 | 0 | 0 | 0.3 | 2.52 | 5.26 | 10 |
| pev26d1_1.6_6 | 79.02 | 0.63 | 11.06 | 0.61 | 0 | 0 | 0 | 0 | 0 | 0 | 0.32 | 2.64 | 5.72 | 10 |
| pev26d1_1.6_7 | 79.28 | 0.58 | 10.76 | 0.84 | 0 | 0 | 0 | 0 | 0 | 0 | 0.44 | 2.72 | 5.38 | 10 |
| pev26d1_1.6_8 | 78.98 | 0.43 | 11.1 | 0.77 | 0 | 0 | 0 | 0 | 0 | 0 | 0.26 | 2.45 | 6.02 | 10 |
| pev26d1_1.8_1 | 78.77 | 0.48 | 11.09 | 0.96 | 0 | 0 | 0 | 0 | 0 | 0 | 0.37 | 2.59 | 5.74 | 10 |
| pev26d1_1.8_2 | 78.36 | 0.61 | 11.07 | 1.2 | 0 | 0 | 0 | 0.17 | 0 | 0 | 0.4 | 2.52 | 5.67 | 10 |
| pev26d1_1.8_3 | 78.61 | 0.62 | 11.21 | 0.97 | 0 | 0 | 0 | 0.26 | 0 | 0 | 0.41 | 2.41 | 5.5 | 10 |
| pev26d1_1.9_1 | 78.43 | 0.52 | 11.3 | 0.73 | 0 | 0 | 0.2 | 0 | 0 | 0 | 0.39 | 2.68 | 5.74 | 10 |
| pev26d1_1.9_2 | 79.44 | 0.53 | 10.83 | 0.79 | 0 | 0 | 0 | 0 | 0 | 0 | 0.37 | 2.61 | 5.41 | 10 |
| pev26d1_1.9_3 | 75.82 | 0.4 | 13.5 | 0.79 | 0 | 0 | 0 | 0 | 0 | 0 | 2.03 | 3.11 | 4.34 | 10 |
| pev26d1_1.9_4 | 78.1 | 0.69 | 11.29 | 1.09 | 0 | 0 | 0 | 0.13 | 0 | 0 | 0.53 | 2.53 | 5.65 | 10 |
| pev26d1_1.9_5 | 78.99 | 0.51 | 10.86 | 0.92 | 0 | 0 | 0 | 0 | 0 | 0 | 0.46 | 2.51 | 5.75 | 10 |
| pev26d1_1.9_6 | 75.86 | 0 | 13.94 | 0.64 | 0 | 0 | 0 | 0 | 0 | 0 | 3.17 | 3.41 | 2.98 | 10 |
| pev26d1_1.9_7 | 75.31 | 0.37 | 13.86 | 0.73 | 0 | 0 | 0 | 0 | 0 | 0 | 2.4 | 3.53 | 3.82 | 10 |
| pev26d1_1.10_1 | 78.88 | 0.44 | 11.22 | 0.86 | 0 | 0 | 0 | 0 | 0 | 0 | 0.34 | 2.59 | 5.66 | 10 |

| | | | | | | | | | | | | | | |
|---|---|---|---|---|---|---|---|---|---|---|---|---|---|---|
| pev26d1_1.10_2 | 78.03 | 0.66 | 11.55 | 0.92 | 0 | 0 | 0 | 0 | 0 | 0 | 0.28 | 2.66 | 5.91 | 10 |
| pev26d1_1.11_2 | 77.45 | 0.6 | 11.74 | 1.08 | 0 | 0 | 0 | 0 | 0 | 0 | 0.41 | 2.61 | 6.11 | 10 |
| pev26d1_1.11_3 | 77.93 | 0.65 | 11.46 | 0.99 | 0 | 0 | 0 | 0 | 0 | 0 | 0.4 | 2.61 | 5.96 | 10 |
| pev26d1_1.11_4 | 77.43 | 0.57 | 11.46 | 1.25 | 0 | 0 | 0 | 0 | 0 | 0 | 0.46 | 2.53 | 6.31 | 10 |
| pev26d1_1.11_5 | 78.14 | 0.61 | 11.41 | 0.87 | 0 | 0 | 0 | 0 | 0 | 0 | 0.29 | 2.68 | 6 | 10 |
| pev26d1_1.11_6 | 79.17 | 0.73 | 10.74 | 0.86 | 0 | 0 | 0 | 0 | 0 | 0 | 0.44 | 2.38 | 5.67 | 10 |
| pev26d1_1.11_7 | 78.7 | 0.61 | 11.05 | 0.96 | 0 | 0 | 0 | 0 | 0 | 0 | 0.37 | 2.46 | 5.85 | 10 |
| pev26d1_1.12_1 | 78.34 | 0.5 | 11.47 | 1.04 | 0 | 0 | 0 | 0 | 0 | 0 | 0.27 | 2.64 | 5.75 | 10 |
| pev26d1_1.12_2 | 78.34 | 0.56 | 11.15 | 1.06 | 0 | 0 | 0 | 0 | 0 | 0 | 0.56 | 2.63 | 5.7 | 10 |
| pev26d1_1.12_3 | 77.38 | 0.69 | 11.67 | 1.04 | 0 | 0 | 0 | 0.13 | 0 | 0 | 0.56 | 2.72 | 5.81 | 10 |
| pev26d1_1.12_4 | 78.38 | 0.63 | 11.3 | 1.07 | 0 | 0 | 0 | 0 | 0 | 0 | 0.37 | 2.6 | 5.65 | 10 |
| pev26d1_1.13_1 | 78.27 | 0.62 | 11.16 | 1.03 | 0 | 0 | 0 | 0 | 0 | 0 | 0.46 | 2.66 | 5.8 | 10 |
| pev26d1_1.13_2 | 78.27 | 0.42 | 11.83 | 0.76 | 0 | 0 | 0 | 0 | 0 | 0 | 1.02 | 2.72 | 4.98 | 10 |
| pev26d1_1.14_1 | 76.93 | 0.54 | 12.06 | 1.2 | 0 | 0 | 0 | 0 | 0 | 0 | 0.47 | 2.86 | 5.94 | 10 |
| pev26d1_1.14_2 | 78.09 | 0.53 | 11.47 | 0.98 | 0 | 0 | 0 | 0 | 0 | 0 | 0.46 | 2.59 | 5.88 | 10 |
| pev26d1_1.14_3 | 77.95 | 0.66 | 11.33 | 0.86 | 0 | 0 | 0 | 0 | 0 | 0 | 0.36 | 2.72 | 6.12 | 10 |
| pev26d1_1.14_4 | 79.77 | 0.57 | 10.69 | 0.84 | 0 | 0 | 0 | 0 | 0 | 0 | 0.39 | 2.43 | 5.3 | 10 |
| pev26d1_1.14_5 | 77.92 | 0.64 | 11.53 | 1.02 | 0 | 0 | 0 | 0 | 0 | 0 | 0.35 | 2.7 | 5.85 | 10 |
| pev26d1_1.15_1 | 78.43 | 0.71 | 10.74 | 1.58 | 0 | 0 | 0 | 0 | 0 | 0 | 0.46 | 2.58 | 4.96 | 10 |
| pev26d1_1.15_3 | 79.35 | 0.51 | 10.89 | 0.82 | 0 | 0 | 0 | 0 | 0 | 0 | 0.42 | 2.51 | 5.51 | 10 |
| pev26d1_1.15_4 | 79.19 | 0.57 | 11.06 | 0.78 | 0 | 0 | 0 | 0 | 0 | 0 | 0.36 | 2.62 | 5.41 | 10 |
| pev26d1_1.16_1 | 77.42 | 0.39 | 11.93 | 1.1 | 0 | 0 | 0 | 0 | 0 | 0 | 0.87 | 2.92 | 5.37 | 10 |
| pev26d1_1.16_2 | 79.66 | 0.28 | 11.14 | 0.63 | 0 | 0 | 0 | 0 | 0 | 0 | 0.47 | 2.73 | 5.1 | 10 |
| pev26d1_1.16_3 | 79.55 | 0.35 | 10.73 | 0.8 | 0 | 0 | 0 | 0 | 0 | 0 | 0.52 | 2.52 | 5.52 | 10 |
| pev26d1_1.16_4 | 79.32 | 0.43 | 11.07 | 0.61 | 0 | 0 | 0 | 0 | 0 | 0 | 0.58 | 2.72 | 5.26 | 10 |
| pev26d1_1.18_1 | 80.5 | 0.68 | 10.17 | 0.71 | 0 | 0 | 0 | 0 | 0 | 0 | 0.34 | 2.47 | 5.13 | 10 |
| pev26d1_1.18_2 | 78.01 | 0.54 | 11.67 | 0.81 | 0 | 0 | 0 | 0 | 0 | 0 | 0.9 | 2.72 | 5.35 | 10 |
| pev26d1_1.18_3 | 79.71 | 0.45 | 10.6 | 0.91 | 0 | 0 | 0 | 0 | 0 | 0 | 0.3 | 2.45 | 5.57 | 10 |
| pev26d1_1.18_4 | 77.02 | 0.4 | 11.79 | 1.42 | 0 | 0 | 0 | 0.18 | 0 | 0 | 0.96 | 2.65 | 5.59 | 10 |
| pev26d1_1.18_5 | 79.26 | 0.42 | 11.11 | 0.72 | 0 | 0 | 0 | 0 | 0 | 0 | 0.61 | 2.82 | 5.07 | 10 |
| pev26d1_1.19_1 | 78.41 | 0.55 | 11.38 | 0.71 | 0 | 0 | 0 | 0 | 0 | 0 | 0.42 | 2.62 | 5.91 | 10 |

| | | | | | | | | | | | | | | |
|---|---|---|---|---|---|---|---|---|---|---|---|---|---|---|
| pev26d1_1.19_2 | 79.28 | 0.51 | 10.89 | 0.79 | 0 | 0 | 0 | 0 | 0 | 0 | 0.38 | 2.52 | 5.63 | 10 |
| pev26d1_1.19_3 | 79.16 | 0.41 | 10.86 | 0.98 | 0 | 0 | 0 | 0 | 0 | 0 | 0.42 | 2.44 | 5.74 | 10 |
| pev26d1_1.19_4 | 78.99 | 0.6 | 11.35 | 0.68 | 0 | 0 | 0 | 0 | 0 | 0 | 0.6 | 2.58 | 5.2 | 10 |
| pev26d1_1.19_5 | 79.44 | 0.42 | 10.72 | 0.9 | 0 | 0 | 0 | 0 | 0 | 0 | 0.43 | 2.59 | 5.5 | 10 |
| pev26d1_1.20_1 | 79.44 | 0.56 | 10.92 | 0.71 | 0 | 0 | 0 | 0 | 0 | 0 | 0.5 | 2.5 | 5.37 | 10 |
| pev26d1_1.20_2 | 79.23 | 0.41 | 11.14 | 0.79 | 0 | 0 | 0 | 0 | 0 | 0 | 0.69 | 2.59 | 5.14 | 10 |
| pev26d1_1.20_3 | 78.21 | 0.44 | 11.67 | 0.76 | 0 | 0 | 0 | 0 | 0 | 0 | 0.84 | 3.03 | 5.05 | 10 |
| pev26d1_1.20_4 | 79.42 | 0.56 | 10.95 | 0.64 | 0 | 0 | 0 | 0 | 0 | 0 | 0.82 | 2.67 | 4.94 | 10 |
| pev26d1_1.20_5 | 78.14 | 0.35 | 11.73 | 1.09 | 0 | 0 | 0 | 0 | 0 | 0 | 1.2 | 2.76 | 4.72 | 10 |
| pev26d1_1.20_6 | 78.45 | 0.51 | 11.39 | 0.87 | 0 | 0 | 0 | 0 | 0 | 0 | 0.7 | 2.74 | 5.33 | 10 |
| pev26d1_1.21_1 | 77.76 | 0.62 | 11.92 | 0.74 | 0 | 0 | 0 | 0 | 0 | 0 | 0.71 | 2.79 | 5.46 | 10 |
| pev26d1_1.21_2 | 78.15 | 0.49 | 11.56 | 0.91 | 0 | 0 | 0 | 0 | 0 | 0 | 0.56 | 2.69 | 5.64 | 10 |
| pev26d1_1.21_3 | 77.5 | 0.58 | 11.73 | 1.09 | 0 | 0 | 0 | 0 | 0 | 0 | 0.59 | 2.9 | 5.61 | 10 |
| pev26d1_1.21_4 | 78.54 | 0.51 | 11.17 | 0.86 | 0 | 0 | 0 | 0 | 0 | 0 | 0.29 | 2.63 | 6 | 10 |
| pev26d1_1.22_1 | 78.62 | 0.54 | 11.18 | 1.01 | 0 | 0 | 0 | 0 | 0 | 0 | 0.43 | 2.67 | 5.56 | 10 |
| pev26d1_1.22_2 | 76.69 | 0.67 | 11.73 | 1.37 | 0 | 0 | 0 | 0.25 | 0 | 0 | 0.41 | 2.65 | 6.23 | 10 |
| pev26d1_1.22_3 | 77.07 | 0.46 | 12.4 | 0.86 | 0 | 0 | 0 | 0 | 0 | 0 | 1.21 | 3.04 | 4.97 | 10 |
| pev26d1_1.22_4 | 77.85 | 0.67 | 11.34 | 1.29 | 0 | 0 | 0 | 0 | 0 | 0 | 0.39 | 2.45 | 6.01 | 10 |
| pev26d1_1.22_5 | 78.73 | 0.59 | 11.16 | 0.88 | 0 | 0 | 0 | 0 | 0 | 0 | 0.43 | 2.53 | 5.69 | 10 |
| pev26d1_1.22_6 | 78.76 | 0.49 | 11.05 | 0.96 | 0 | 0 | 0 | 0 | 0 | 0 | 0.42 | 2.59 | 5.72 | 10 |
| pev26d1_1.22_7 | 78.57 | 0.43 | 11.58 | 0.78 | 0 | 0 | 0 | 0 | 0 | 0 | 0.96 | 2.87 | 4.82 | 10 |
| pev26d1_1.23_1 | 77.81 | 0.55 | 11.61 | 1.02 | 0 | 0 | 0 | 0 | 0 | 0 | 0.41 | 2.63 | 5.97 | 10 |
| pev26d1_1.23_2 | 77.72 | 0.56 | 11.57 | 1.04 | 0 | 0 | 0 | 0.16 | 0 | 0 | 0.67 | 2.73 | 5.56 | 10 |
| pev26d1_1.23_3 | 81.12 | 0.49 | 9.93 | 0.66 | 0 | 0 | 0 | 0 | 0 | 0 | 0.33 | 2.47 | 5.01 | 10 |
| PEV26G_2_2_13 | 65.94 | 0.49 | 17.51 | 0 | 0 | 2.63 | 0 | 1.51 | 0 | 0 | 3.17 | 4.01 | 4.46 | 10 |
| PEV26G_2_5_5 | 63.58 | 1.04 | 17.64 | 0 | 0 | 2.66 | 0 | 0.47 | 0 | 0 | 1 | 3.79 | 8.93 | 10 |
| PEV26I_1.1_2 | 77.74 | 0 | 12.29 | 0.97 | 0 | 0 | 0 | 0 | 0 | 0 | 1.12 | 2.93 | 4.95 | 10 |
| PEV26I_1.1_4 | 71.99 | 0 | 16.57 | 0.63 | 0 | 0 | 0 | 0 | 0 | 0 | 3.59 | 4.33 | 2.9 | 10 |
| PEV26I_1.2_1 | 75.66 | 0 | 14.17 | 0.67 | 0 | 0 | 0 | 0 | 0 | 0 | 2.1 | 3.48 | 3.93 | 10 |
| PEV26I_1.2_2 | 79.63 | 0 | 11.18 | 0.72 | 0 | 0 | 0 | 0 | 0 | 0 | 0.52 | 2.35 | 5.61 | 10 |
| PEV26I_1.2_3 | 79.53 | 0.74 | 10.95 | 0.59 | 0 | 0 | 0 | 0 | 0 | 0 | 0 | 2.34 | 5.84 | 10 |

| | | | | | | | | | | | | | |
|---|---|---|---|---|---|---|---|---|---|---|---|---|---|
| PEV26I_1.2_4 | 71.94 | 1 | 12.33 | 4.49 | 0 | 0 | 0 | 0.77 | 0 | 0 | 2.95 | 3.12 | 3.41 | 10 |
| PEV26I_1.2_5 | 78.82 | 0 | 11.69 | 0.94 | 0 | 0 | 0 | 0 | 0 | 0 | 1.05 | 2.74 | 4.75 | 10 |
| PEV26I_1.2_6 | 78.51 | 0 | 11.94 | 0.72 | 0 | 0 | 0 | 0 | 0 | 0 | 1.49 | 3.09 | 4.24 | 10 |

**Table 4.** Paraná magma-meter results (top) and compositions (bottom). If the magma-meter was not able to calculate a triple-junction, there is a "-" symbol. Note that only one composition has yielded a triple-junction thus far. The $f_{O2}$ and $H_2O$ ranges represent those that were tested for the magma-meter.

>1,000,000 km$^3$ of basaltic Serra Geral Formation (Frank et al 2009). The modes of eruption and deposition of the silicic deposits have proven elusive (Peate, 1997), but fieldwork by our group over recent years has led to the recognition of both effusive dome structures, as well as explosive deposits now exposed along terraces (Gravely et al, 2015; Tramontano et al., 2014).

Within the Palmas unit, there are several observed outcrops of juvenile lenticular structures (informally called "Barbosas"), which appear to maintain their pre-eruptive cohesive properties, similar to fiamme (Gravley et al. 2015). The fiamme-like Barbosas outcrop in explosive ignimbrite deposits in oriented swarms, and range in thickness from several mm to ~30 cm (Tramontano et al, 2014). The Barbosas contain variably altered glass and have a plag+opx+cpx mineral assemblage, so are viable for application to the magma-meter. Unlike the pristine glass from Ruapehu pumice, the glass in the Paraná Barbosas is somewhat devitrified and silicified, so large swathes of usable glass are difficult to analyze. Instead of averaging glass analyses, we run magma-meter calculations on individual glass compositions to model storage conditions.

*Preliminary Results from Paraná Palmas Unit:*

Thus far, we have tested the magma-meter on one outcrop, and have modeled many individual glass compositions from each of the 5 Barbosas, Table 4. Of the 153 glass compositions modeled, 1 magma-meter calculations produced a triple-junction, Table 4. Like the Ruapehu results, the Paraná Barbosas triple-junction is at ΔQFM ~1-1.5 and is water-saturated. The triple-junction pressure is quite low, 90 MPa. The sparse results from Paraná reflect the difficulty in determining the glass compositions from the somewhat altered glass. We are currently working on finding additional viable glass compositions in other samples from the Paraná Volcanics.

**Conclusions and Future Work:**

In this work, we develop a "magma-meter" for rocks containing the assemblage plag+opx+cpx. The immediate outcome of this model is to determine the conditions, particularly pressure, temperature, $H_2O$ wt.%, and $f_{O2}$, at which magma is stored and crystallizes prior to eruption. We test the magma-meter with experiments from the literature, and we show that: (1) most experiments do not yield viable conditions for the coexistence of plag+opx+cpx with melt of the given composition; (2) when conditions are calculated by the magma-meter, the results are consistent with experimental conditions. This suggests that, when successful, the magma-meter retrieves appropriate conditions. We use the magma-meter to constrain storage conditions of magmas from Mt Ruapehu, New Zealand and Paraná Palmas Unit, Brazil, which shows that the magma-meter can inform us about active magma systems as well as extinct systems. Our results for Mt Ruapehu suggest a correlation between pre-eruptive magma storage conditions and eruption style.

The magma-meter can be run using a new version MELTS_Excel (Gualda and Ghiorso, 2015), which will be made available on the rhyolite-MELTS website.

# REFERENCES

Auwera J.V., Longhi J. (1994) Experimental study of a jotunite: constraints on the parent magma composition and crystallization conditions (P, T, $f_{O2}$) of the Bjerkreim-Sokndal layered intrusion (Norway). Contributions to Mineralogy and Petrology: v. 118, p. 60-78.

Baker L.L., Rutherford M.J. (1996) The effect of dissolved water on the oxidation state of silicic melts. Geochimica et Cosmochimica Acta: v. 60, p. 2179–2187.

Bégué F., Pamukcu A.S., Gualda G.A.R., Ghiorso M.S., Gravley D.M., Deering C.D. (2014) Phase-equilibrium geobarometers for silicic rocks based on rhyolite-MELTS. Part 2: Application to Taupo Volcanic Zone rhyolites. Contributions to Mineralogy and Petrology: v. 168, p. 1082.

Blundy J., Cashman K. (2008) Petrologic reconstruction of magmatic system variables and processes. Reviews in Mineralogy and Geochemistry: v. 69, p. 179-239.

Bryan S.E., Ukstins Peate I.A., Self S., Peate D., Jerram D.A., Mawby M.R., Miller J., and Marsh J.S. (2010) The largest volcanic eruptions on Earth. Earth Science Reviews: v. 02, p. 207–229.

Cashman K.V., Giordano G. (2014) Calderas and magma reservoirs. Journal of Volcanology and Geothermal Research: v. 288, p. 28-45.

Cowlyn J.D. (2016) Pyroclastic density currents at Ruapehu volcano; New Zealand. University of Canterbury.

Ferry J.M., Watson E.B. (2007) New thermodynamic models and revised calibrations for the Ti-in-zircon and Zr-in-rutile thermometers. Contributions to Mineralogy and Petrology: v. 154, p. 429-437.

Frank H.T., Gomes M.E.B., Formoso M.L.L. (2009) Review of the areal extent and the volume of the Serra Geral Formation, Paraná Basin, South America. Pesquisas em Geociências: v. 36, p. 49-57.

Ghiorso M.S., Evans B.W. (2008) Thermodynamics of rhombohedral oxide solid solutions and a revision of the Fe–Ti two-oxide geothermometer and oxygen- barometer. American Journal of Science: v. 308, p. 957–1039.

Gravely D.M., Gualda G.A.R., Harmon L.J., Tramontano S., Luchetti A.C.F., Nardy A. (2015) Zooming into the Paraná-Etendeka silicic volcanics, southern Brasil: a physical volcanological approach. American Geophysical Union: T32D-08.

Grove T.L., Donnelly-Nolan J.M., Housh T. (1997) Magmatic processes that generated the rhyolite of Glass Mountain, Medicine Lake volcano, N. California. Contributions to Mineralogy and Petrology: v. 127, p. 205-223.

Gualda G.A.R., Ghiorso M.S. (2014) Phase-equilibrium geobarometers for silicic rocks based on rhyolite-MELTS. Part 1: Principles, procedures, and evaluation of the method. Contributions to Mineralogy and Petrology: v. 168, no. 1, p. 1033.

Gualda G.A.R., Ghiorso M.S. (2015) MELTS_Excel: A Microsoft Excel-based MELTS interface for research and teaching of magma properties and evolution. Geochemistry, Geophysics, Geosystems: v. 16, no. 1, p. 315–324.

Hackett W.R., Houghton B.F. (1989) A facies model for a Quaternary andesitic composite volcano: Ruapehu, New Zealand. Bulletin of Volcanology: v. 51, p. 51-68.

Hawkesworth C.J., Gallagher K., Kirstein L., Mantovani M.S.M., Peate D.W., Turner S.P. (2000) Tectonic controls on magmatism associated with continental break-up: an example from the Paraná-Etendeka Province. Earth and Planetary Science Letters: v. 179, p. 335-349.

Holland T. J. B., Powell R. (2006) Mineral activity-composition relations and petrological calculations involving cation equipartition in multisite minerals: a logical inconsistency. Journal of Metamorphic Geology: v. 24, no. 9, p. 851-861.

Kawamoto T. (1996) Experimental constraints on differentiation and $H_2O$ abundance of calc-alkaline magmas. Earth and Planetary Science Letters: v. 144, p. 577-589.

Kilinc A., Carmichael I.S.E., Rivers M.L., Sack R.O. (1983) The ferric–ferrous ratio in natural silicate liquids equilibrated in air. Contributions to Mineralogy and Petrology: v. 83, p. 136–140.

Kress V.C., Carmichael I.S.E. (1991) The compressibility of silicate liquids containing Fe2O3 and the effect of composition, temperature, oxygen fugacity and pressure on their redox states. Contributions to Mineralogy and Petrology: v. 108, p. 82–92.

Lange R.A., Carmichael I.S.E. (1987) Densities of Na2O–K2O–CaO–MgO–FeO–Fe2O3–Al2O3–TiO2–SiO2 liquids: new measurements and derived partial molar properties. Geochimica et Cosmochimica Acta: v. 51, p. 2931–2946.

Lange R.A., Frey H.M., Hector J. (2009) A thermodynamic model for the plagioclase-liquid hygrometer/thermometer. American Mineralogist: v. 94, p. 494-506.

Liebske C., Behrens H., Holtz F., Lange R.A. (2002) The influence of pressure and composition on the viscosity of andesitic melts. Geochimica et Cosmochimica Acta: v. 67, p. 473–485.

Liu Y., Zhang Y., Behrens H. (2005) Solubility of $H_2O$ in rhyolitic melts at low pressures and a new empirical model for mixed $H_2O$-$CO_2$ solubility in rhyolitic melts. Journal of Volcanology and Geothermal Research: v. 143, p. 219–225.

Moore G. (2008) Interpreting $H_2O$ and $CO_2$ contents in melt inclusions: constraints from solubility experiments and modeling. Reviews in Mineralogy and Geochemistry: v. 69, p. 333-361.

Moore G., Carmichael I.S.E. (1998) The hydrous phase equilibria (to 3 kbar) of an andesite and basaltic andesite from western Mexico: constraints on water content and conditions of phenocryst growth. Contributions to Mineralogy and Petrology: v. 130, p. 304-319.

Moore G., Righter K., Carmichael I.S.E. (1995) The effect of dissolved water on the oxidation state of iron in natural silicate liquids. Contributions to Mineralogy and Petrology: v. 120, p. 170–179.

Mysen B.O. (1990) Relationships between silicate melt structure and petrologic processes. Earth-Science Reviews: v. 27, p. 281–365.

Mysen B.O., Virgo D., Neumann E.R., Seifert F.A. (1985) Redox equilibria and the structural states of ferric and ferrous iron in melts in the system CaO–MgO–Al2O3–SiO2– Fe–O; relationships between redox equilibria, melt structure and liquidus phase equilibria. American Mineralogist: v. 70, p. 317–331.

Nardy A.J.R., Rosa M.C., Luchetti A.C.F., Ferreira M.L.C., Machado F.B., Oliveira M.A.F. (2011) Parâmetros físicos pré-eruptivos do magmatismo ácido da provincial magmatica do Paraná: resultados preliminares. Geociências, v. 30, p. 575-588.

Pamukcu A.S., Gualda G.A.R., Ghiorso M.S., Miller C.F. (2015) Phase-equilibrium geobarometers for silicic rocks based on rhyolite-MELTS. Part 3: Application to the Peach Spring Tuff (Arizona-California-Nevada, USA). Contributions to Mineralogy and Petrology: v. 169, p. 33.

Peate D.W. (1997) The Paraná-Etendeka Province. In: J Mahoney & M Coffin (eds), Large Igneous Provinces: Continental, Oceanic, and Planetary Flood Volcanism: AGU Geophysical Monograph: v. 100, p. 217-245.

Prouteau G., Scaillet B. (2003) Experimental constraints on the origin of the 1991 Pinatubo dacites. Journal of Petrology: v. 44, p. 2203-2241.

Putirka K.D. (2008) Thermometers and barometers for volcanic systems. Reviews in Mineralogy and Geochemistry: v. 69, p. 61-120.

Rowland J.V., Sibson R.H. (2001) Extensional fault kinematics within the Taupo Volcanic Zone, New Zealand: soft-linked segmentation of a continental rift system. New Zealand Journal of Geology and Geophysics: v. 44, p. 271–283.

Rowland J.V., Wilson C.J.N., Gravley D.M., (2010) Spatial and temporal variations in magma-assisted rifting, Taupo Volcanic Zone, New Zealand. Journal of Volcanology and Geothermal Research: v. 190, p. 89–108.

Sack R.O., Carmichael I.S.E., Rivers M., Ghiorso M.S. (1980) Ferric–ferrous equilibria in natural silicate liquids at 1 bar. Contributions to Mineralogy and Petrology: v. 75, p. 369–376.

Sack R.O., Ghiorso M.S. (1991) Chromium spinels as petrogenetic indicators: thermodynamics and petrological applications. American Mineralogist: v. 87, p. 79-98.

Toplis M.J., Carrol M.R. (1995) An experimental study of the influence of oxygen fugacity on Fe–Ti–oxide stability, phase relations and mineral–melt equilibria in ferrobasaltic systems. Journal of Petrology: v. 36, p. 1137–1170.

Tramontano S. (2016) The importance of minerals and bubbles: (1) The internal trigger test: mapping overpressure regimes for giant magma bodies (2) Developing and incorporating instructional videos and quizzes as a blended and online learning component in an undergraduate optical microscopy curriculum. Vanderbilt University: ch. 1.

Tramontano S., Harmon L.J., Gravley D.M., Gualda G.A.R. (2014) New field evidence for silicic ignimbrites and proximal lavas and their distribution in the Paraná Basin, Brazil. AGU Fall Meeting: V21B-4754.

Wark D.A., Watson E.B. (2006) TitaniQ: a titanium-in-quartz geothermometers. Contributions to Mineralogy and Petrology: v. 152, p. 743-754.

Waters L.E., Lange R.A. (2015) An updated calibration of the plagioclase-liquid hygrometer-thermometer applicable to basalts through rhyolites. American Mineralogist: v. 100, p. 2172-2184.

Wilson C.J.N., Houghton B.F., McWilliams M.O., Lanphere M.A., Weaver S.D., Briggs R.M., (1995) Volcanic and structural evolution of Taupo Volcanic Zone, New Zealand: a review. Journal of Volcanology and Geothermal Research: v. 68, p. 1–28.